JOURNAL OF Materials CHEMISTRY

# Formation of 2:1 insulating complexes of $D^{+\cdot}D^{+\cdot}A^{2-}$ alternating stack and a 4:1 semimetallic complex using $M(dto)_2$ dianions (M = Ni, Pd or Pt and dto = dithiooxalate)†

**Gunzi Saito,*[a] Hiroko Izukashi,[a] Michihiro Shibata,[a] Keisuke Yoshida,[a] Lyudmila A. Kushch,‡[a] Tetsuo Kondo,§[a] Hideki Yamochi,§[a] Olga O. Drozdova,¶[a] Kiyoshi Matsumoto,[b] Masami Kusunoki,[c] Ken-ichi Sakaguchi,[c] Norimichi Kojima[d] and Eduard B. Yagubskii[e]**

[a]*Division of Chemistry, Graduate School of Science, Kyoto University, Sakyo-ku, Kyoto 606-8502, Japan. E-mail: saito@kuchem.kyoto-u.ac.jp*
[b]*Graduate School of Human and Environment Studies, Kyoto University, Sakyo-ku, Kyoto 606-8501, Japan*
[c]*Institute for Protein Research, Osaka University, Suita, Osaka 565-0871, Japan*
[d]*Department of Pure and Applied Sciences, College of Arts and Sciences, University of Tokyo, Komaba, Meguro-ku, Tokyo 153-8902, Japan*
[e]*Institute of Problems of Chemical Physics, Russian Academy of Sciences, 142432, Chernogolovka, Moscow District, Russia*

***Received 1st November 1999, Accepted 19th January 2000***

The preparation of charge transfer (CT) complexes of dithiooxalate (dto) transition metal salts $M(dto)_2$ (M = Ni, Pd, Pt or Cu) with a variety of electron donor molecules was examined based on the redox properties of constituent molecules. Conventional electron donors of TTF type, such as bis(ethylenedithio)- (BEDT-TTF (ET)) and bis(ethylenedioxy)-tetrathiafulvalene (BEDO-TTF (BO)), mainly afford 2:1 solid CT complexes composed of a donor cation dimer $D^{+\cdot}D^{+\cdot}$ and dianion of $M(dto)_2$ ($A^{2-}$) when M = Ni, Pd or Pt. The constituent molecules stack alternately to construct a $D^{+\cdot}D^{+\cdot}A^{2-}$ column. Their crystal structures are unique among the ET and BO complexes so far known, namely the $M(dto)_2^{2-}$ ions are isolated from each other being surrounded by six dimers of $D^{+\cdot}$ in the crystals. Three kinds of 2:1 complex were obtained between ET and $Pd(dto)_2$. The electronic spectra of the solids are characterized by the particular intradimer transition of the donor cation dimer. The infrared vibrational spectra strongly exhibit the $a_g$ modes of the donor cation due to its dimerization. All of the complexes are electrical insulators. A singlet–triplet magnetic excitation is clearly observed for some of them. A highly conductive 4:1 complex was obtained between ET and $Pd(dto)_2$, $(ET)_4[Pd(dto)_2]$, which exhibited electronic absorption extending below $5\times10^3$ cm$^{-1}$. The complex shows a semimetallic nature.

## 1 Introduction

Several dithiolene ligand (DTL)–transition metal (M) systems are known to form interesting charge transfer (CT) complexes with π-electron donors (D) or acceptors (A). The systems and molecules discussed in this paper are depicted in Fig. 1. Prior to the discovery of the molecular metals and superconductors based on $M(dmit)_2$,[1] the systems $M(edt)_2$, $M(mnt)_2$ and $M(thiete)_2$ afforded many attractive materials, *i.e.* highly conductive salts and organic metals, *e.g.* $NH_4[Ni(mnt)_2]\cdot1.15H_2O$,[2] $Li_{0.75}[Pt(mnt)_2]\cdot2H_2O$,[3] $(perylene)_2[M(mnt)_2]$,[4] spin-Peierls system, *e.g.* $(TTF)_2[Cu(thiete)_2]$,[5] disordered solid solution, *e.g.* $(TTF)_2[Ni(edt)_2]_3$[6], *etc.* Work has continued on the preparation of new ligands such as dddt[7] and tdas.[8]

Although the transition metal dithiooxalates (dto), $[M(dto)_2]$, have long been known, they were not paid much attention as a source of conducting materials compared with their oxygen analogues, transition metal oxalates (ox) $[M(ox)_n]$. The complex $[Pt(ox)_2]$ gave a variety of cation deficient salts with high conductivity in the 60's and 70's, such as $K_{1.64}[Pt(ox)_2]\cdot H_2O$ ($\sigma_{RT}\approx42$ S cm$^{-1}$) and $Mg_{0.82}[Pt(ox)_2]\cdot5.3H_2O$ (50 S cm$^{-1}$),[9] where $\sigma_{RT}$ is the conductivity at room temperature (RT).

Propeller-shaped tris(oxalato)metalate anions $[M(ox)_3]$ (M = Si, Ge or Sn) and planar bis(oxalato)metalate anions $[M(ox)_2]$ (M = Cu or Pt) were used as counter anions for formation of semiconductive CT complexes of TTF and TSF ($\sigma_{RT}=10^{-3}$–$10^{-5}$ S cm$^{-1}$).[10] Soon metallic complexes of BEDT-TTF (ET), *i.e.* $(ET)_4[Pt(ox)_2]$,[11–14] $(ET)_4[Cu(ox)_2]$,[15,16] and superconducting β″-$(ET)_4[Fe(ox)_3]\cdot H_3O\cdot PhCN$,[17] were prepared and their structures and transport properties studied.

Contrary to the oxalate system, the $M(dto)_2$ system has not afforded metal deficient compounds but the commensurate ones with potassium. They were insulators ($\sigma_{RT}=1\times10^{-9}$ (M = Ni), $8\times10^{-8}$ (Pd), $6\times10^{-10}$ S cm$^{-1}$ (Pt)).[18] $[Ni(dto)_2]^{2-}$ was oxidized by iodine vapor and reported to show metallic temperature dependence near RT (0.5–200 S cm$^{-1}$) in some

†Bond lengths, bond angles and atomic parameters available as supplementary data (ESI). For direct electronic access see http://www.rsc.org/suppdata/jm/a9/a908670f/

‡*Permanent address*: Institute of Problems of Chemical Physics, Russian Academy of Sciences, 142432, Chernoglovka, Moscow District, Russia.

§Also belongs to CREST, Japan Science and Technology Corporation (JST).

¶On leave from A. F. Ioffe Physico-Technical Institute, Russian Academy of Sciences, 194021 St. Petersburg, Russia.

DOI: 10.1039/a908670f

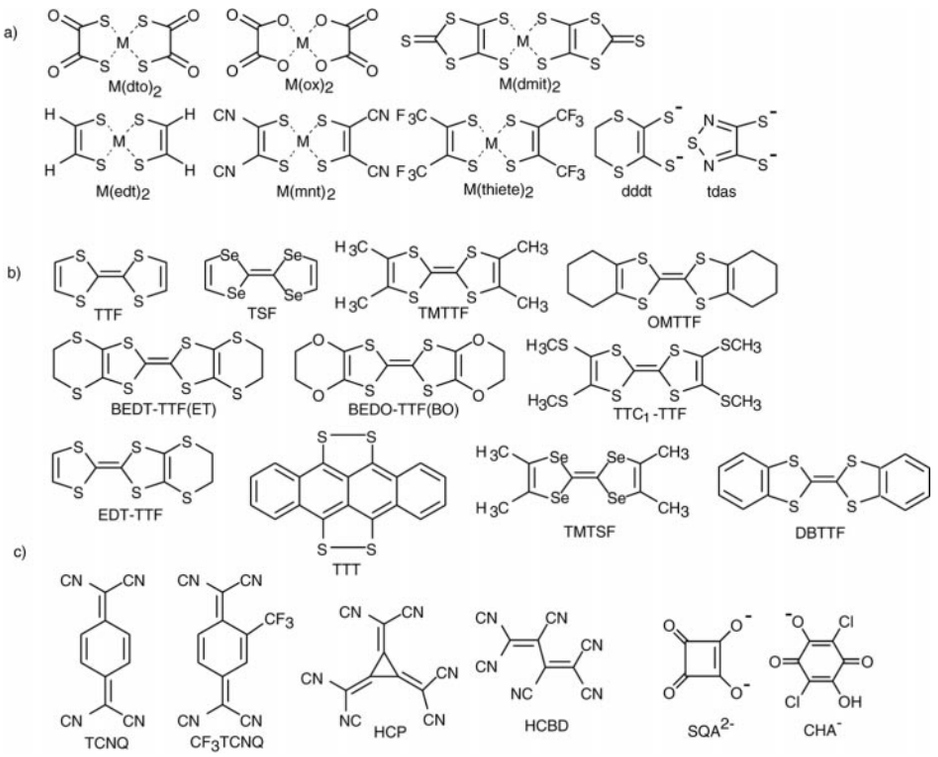


**Fig. 1** Chemicals mentioned: a) ligand or transition metal–ligand system; b) organic electron donor molecules; c) organic electron acceptor molecules.

samples.[18] However, it has been claimed that $K_2[Ni(dto)_2]I$ is not stable and can only be identified in solution but not isolated in the solid state.[19]

Bellitto *et al.* prepared insulating ($\sigma_{RT} < 10^{-5}$ S cm$^{-1}$) kinds of TTF complexes by methathesis between $TTF_3(BF_4)_2$ and $R_2[M(dto)_2]$ (R = tetraethylammonium or tetraphenylarsonium): a 3 : 1 complex $[(TTF^{+\cdot})_2(TTF^0)][Pt(dto)_2]^{2-}$, 2 : 1 complexes $(TTF^{+\cdot})_2[M(dto)_2]^{2-}$ (M = Pt or Pd) where the packing pattern is $D^{+\cdot}D^{+\cdot}A^{2-}$, and a 1 : 1 complex $(TTF^{+\cdot})[Cu(dto)_2]^-$.[20] It is noteworthy that $[Cu(dto)_2]^{2-}$ was easily oxidized by $TTF^{+\cdot}$ to afford $[Cu(dto)_2]^-$ having $Cu^{3+}$ species.[20]

We have been studying the $[M(dto)_2]$ complexes from the following standpoints.[21] (1) $[M(dto)_2]^{2-}$ is a larger anion than $[M(ox)_2]^{2-}$. The geometrical distances between the atoms of $Pt(ox)_2$ and $Ni(dto)_2$ are compared in Table 1.[19,22] The length *a* increases by about 12% from $Pt(ox)_2$ to $Ni(dto)_2$ despite the shrinkage of M. $[M(dto)_2]^{2-}$ is even larger than $[M(CN)_4{\cdot}H_2O]^{2-}$ which affords ET superconductors under pressure.[23] In general a longer anion gives rise to a larger interplanar separation of donor molecules, that will give a poorer conductivity but higher density of states at the Fermi level resulting in a higher critical temperature of superconductivity. (2) The ratio *c* : *b* of $Pt(ox)_2$ (0.96 : 1) is close to unity but that of $Ni(dto)_2$ is considerably larger (1.17 : 1). From a geometrical point of view, the sulfur atoms of $M(dto)_2$ have a much more important role than the inner oxygen of $M(ox)_2$ in the formation of chalcogen–chalcogen atomic contacts along the molecular short axis. (3) The electronic structure of $M(dto)_2$ seems considerably different from that of $M(ox)_2$ as exemplified by both that alkali cation deficiency is observed only in the $Pt(ox)_2$ salts but not in the $M(dto)_2$ (M = Pt or Ni) salts and $[Cu(dto)_2]^{2-}$ is easily oxidized by $TTF^{+\cdot}$ but $[Cu(ox)_2]^{2-}$ is not. (4) By replacing oxygen by sulfur atoms the polarizability of the ligand increases and the coordination ability will be changed since sulfur is softer than oxygen. It has been observed that the outer ethylene groups of an ET molecule tend to form pseudo hydrogen bonds with the anions in many ET complexes.[24] This kind of bond has well been recognized in the $Pt(ox)_2$ and $Cu(ox)_2$ salts of ET, between the CH groups of an ET molecule and oxygen atoms of C=O groups of oxalate.[11,15] Therefore, by replacement of ox by dto, the interaction between a donor especially an ET molecule and an anion will considerably be modified from the viewpoints of atomic contacts.

In this paper we describe the preparation, crystal and molecular structures and physical properties of $M(dto)_2$ electrolytes and some CT complexes of $M(dto)_2$, especially semiconductive 2 : 1 complexes of ET, BO, TMTTF and OMTTF with M = Ni, Pd or Pt and a semimetallic 4 : 1 complex of ET with M = Pd in detail, in order to understand the fundamental features of the $M(dto)_2$ compounds.

**Table 1** Geometrical features of $Pt(ox)_2$ and $Ni(dto)_2$ dianions

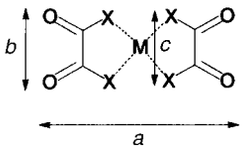


| | $Pt(ox)_2$ | $Ni(dto)_2$ |
|---|---|---|
| Length/Å | M = Pt, X = O | M = Ni, X = S |
| *a* | 7.4 | 8.26 |
| *b* | 2.8 | 2.69 |
| *c* | 2.7 | 3.16 |

## 2 Experimental

$NiCl_2{\cdot}H_2O$, $CuCl_2{\cdot}2H_2O$, $K_2PtCl_4$, $K_2PdCl_4$ and tetraphenylphosphonium (TPP) chloride were used as purchased. Other chemicals were purified by recrystallization, distillation and/or sublimation. The potassium salt of dto, $K_2$dto, was either purchased (Eastman Kodak Co.) or synthesized.[25] Some of the

preparative procedures of each complex are described in each section.

Cyclic voltammetry was obtained in 0.1 M solutions of tetrabutylammonium tetrafluoroborate (TBA·$BF_4$) in $CH_3CN$ with Pt electrodes *vs.* SCE (saturated calomel electrode) at scan speeds of 10–20 mV $s^{-1}$ using a YANACO POLAROGRAPHIC ANALYZER P-1100 at 20–22 °C. Optical measurements were carried out with KBr disks on Perkin-Elmer PARAGON 1000 or 1600 Series instruments in the FT-IR region (400–7800 $cm^{-1}$) and on a SHIMADZU UV-3100 spectrometer for near-infrared, visible and ultraviolet (UV-VIS-NIR) regions (3800–42 000 $cm^{-1}$).

The stoichiometries of complexes were determined by crystal structure analysis and/or density measurement of single crystals and/or elemental analysis. The densities of crystals were determined by the floating method in a mixture of carbon tetrachloride and 1,2-dibromoethane. The intensity data of the structural analysis were collected on an automatic four circle diffractometer or oscillator type X-ray imaging plate with monochromated Mo-K$\alpha$ radiation at RT. The structures were solved by direct methods using Crystan GM6.3 or SHELXS 86.[26] The refinements were performed by the full matrix least squares method.

CCDC reference number 1145/205.

The band structure calculation was performed by the extended Hückel method with tight binding approximation and single $\zeta$-parameter including d orbitals of sulfur atoms.[27]

DC conductivities were measured with either a standard four- or two-probe technique, using gold paint (Tokuriki No. 8560-1A) by attaching gold wires (10–20 μm diameter) to the samples. For powdered samples, measurements were performed on compressed pellets which were cut to form an orthorhombic shape. Static magnetic susceptibility measurements were done with the aid of a SQUID magnetosusceptometer (Quantum Design MPMS) from 300 to 1.9 K. EPR measurements were performed by a JEOL-TE200 X band EPR spectrometer with an Oxford TE011 cavity from RT to *ca.* 3.0 K with the aid of the Oxford ESR-900 cryostat.

## 3 Supporting electrolyte: $(TPP)_2[M(dto)_2]$

### 3.1 Preparation and UV-VIS-IR Spectra of $[M(dto)_2]$

Table 2 summarizes the color, shape, melting point and IR and UV-VIS spectral data of the electrolytes $(TPP)_2[M(dto)_2]$ (M = Ni, Cu, Pd or Pt). The $K_2[M(dto)_2]$ was prepared according to the literature[25] and purified by recrystallization from distilled water. The IR spectra of $K_2[M(dto)_2]$ (M = Ni,[28,29] Pd,[28] or Pt[30]) were in good agreement with those reported and are shown in the footnote of Table 2. The IR spectrum of $K_2[Ni(dto)_2]$ indicates that the crystal obtained here is the red polymorph.[29]

The TPP salt of $Ni(dto)_2$ was prepared by the addition of a filtered aqueous solution of $K_2(dto)$ to a solution of $NiCl_2·6H_2O$ and TPP·Cl in water (red precipitate, 89.5% yield), then purified by recrystallization from $CH_3CN$ to yield red plates (84.1% yield). The TPP salts of $Pd(dto)_2$, $Pt(dto)_2$ and $Cu(dto)_2$ were prepared in a similar way by using $K_2PdCl_4$, $K_2PtCl_4$ and $CuCl_2·2H_2O$, respectively. $(TPP)_2[Cu(dto)_2]$ was not thermally stable, especially in solution, compared to other salts of M = Ni, Pd or Pt.

Based on the similar appearance of the IR spectra to those of the red and black forms of $K_2[Ni(dto)_2]$[29], the IR bands of $(TPP)_2[Ni(dto)_2]$ were assigned as follows: 1604 (s, $b_{2u}$ $\nu_{12}$, C=O str.), 1583 (m, $b_{3u}$ $\nu_{18}$, C=O str.), 1054 (m, $b_{2u}$ $\nu_{13}$, C–C str. and C–S str.), 914 $cm^{-1}$ (m, $b_{3u}$ $\nu_{19}$, O–C–S tor.) and the others are ascribable to those of the TPP molecule. The Raman spectrum of $K_2[Ni(dto)_2]$ has been reported to show $a_g$ modes at 1602 ($\nu_2$), 1085 ($\nu_1$), 607 $cm^{-1}$ ($\nu_3$), and so on.[29] Even though the first one has a frequency very close to that of $b_{2u}$ $\nu_{12}$ of the IR spectrum, the appearance of the last two modes in the IR spectrum was utilized for an indication of a lattice deformation such as dimerization in the anion.

The UV-VIS spectra of $(TPP)_2[M(dto)_2]$ in KBr are in good agreement with the reported ones of $K_2[M(dto)_2]$ (M = Ni or Pd in $CH_2Cl_2$)[28] and $(TBA)_2[M(dto)_2]$ (M = Ni, Pd or Pt in $CH_3CN$).[31] These absorption bands have been assigned based on molecular orbital calculations.[28,31]

**Table 2** Characteristics of supporting electrolytes $(TPP)_2[M(dto)_2]$ (TPP = tetraphenylphosphonium, M = Ni, Cu, Pd or Pt)

| | Ni | Cu | Pd | Pt |
|---|---|---|---|---|
| Color | Red | Dark green | Yellow | Reddish orange |
| Shape | Plate | Needle | Plate | Plate |
| Mp/°C | 271–273 | 163–165 (decomp.) | 278–284 (decomp.) | 263–266 |
| IR[a] in KBr/$cm^{-1}$ | 1604s | 1610s | 1602s | 1600s |
| | 1583m | 1583m | 1583m | 1584m |
| | 1054m | 1038m | 1052m | 1050m |
| | 914m | 910m | 910m | 916m |
| UV-VIS[b]/$10^3$ $cm^{-1}$ | 17.9 | 17.7 | 25.8 | 18.2(sh) |
| | 19.6 | 24.4 | 35.6 | 20.6(sh) |
| | 27.7(sh) | 30.7 | | 22.8 |
| | 32.6 | 36.7 | | 31.0(sh) |
| | 36.7 | | | 36.3(sh) |

[a] $K_2[Ni(dto)_2]$: 1601, 1582, 1087, 939 (1602, 1585, 1084, 933, 615 $cm^{-1}$ (ref. 29)). $K_2[Pd(dto)_2]$: 1604, 1579, 1085, 935 (1618, 1590, 1048, 913, 614 $cm^{-1}$ (ref. 28)). $K_2[Pt(dto)_2]$: 1584, 1082, 940 (1594, 1083, 939, 573 $cm^{-1}$ (ref. 30)). [b] $K_2[Ni(dto)_2]$: 17.8(sh), 19.9, 32.7 in $CH_2Cl_2$. $K_2[Pd(dto)_2]$: 25.1, 36.4, 41.3 in $CH_2Cl_2$ (ref. 28) (all $\times 10^3$ $cm^{-1}$).

**Table 3** Oxidation peak potentials $E_p^{ox}$ of $(TPP)_2[M(dto)_2]$, several anions and donor TTFs

| Dianion | $E_p^{ox}$/V | Anion | $E_p^{ox}$/V | Cation | $E_p^{red}$/V |
|---|---|---|---|---|---|
| $(TBA^+)_2[Cu(ox)_2]^{2-}$ | +1.33 | $HCBD^-$ | +0.75 | $TMTTF^+$ | +0.26 |
| $(TPP^+)_2[Pd(dto)_2]^{2-}$ | +1.21 | $F_4TCNQ^-$ | +0.64 | $OMTTF^+$ | +0.26 |
| $(TPP^+)_2[Pt(dto)_2]^{2-}$ | +0.90 | $F_2TCNQ^-$ | +0.44 | $TTF^+$ | +0.31 |
| $(TPP^+)_2[Ni(dto)_2]^{2-}$ | +0.57 | $FTCNQ^-$ | +0.35 | $BEDO\text{-}TTF^+$ | +0.40 |
| $(TPP^+)_2[Cu(dto)_2]^{2-}$ | +0.12 | $TCNQ^-$ | +0.26 | $EDT\text{-}TTF^+$ | +0.41 |
| $(TBA^+)_2HCP^{2-}$ | +1.25 | *p*-Chloranil$^-$ | +0.09 | $BEDT\text{-}TTF^+$ | +0.50 |

Oxidation and reduction peak potentials *vs.* SCE, Pt electrode, $CH_3CN$, 0.1 M tetrabutylammonium (TBA)·tetrafluoroborate, 19–22 °C, 10–20 mV $s^{-1}$, for the processes of −2→−1, −1→0 and +1→0.

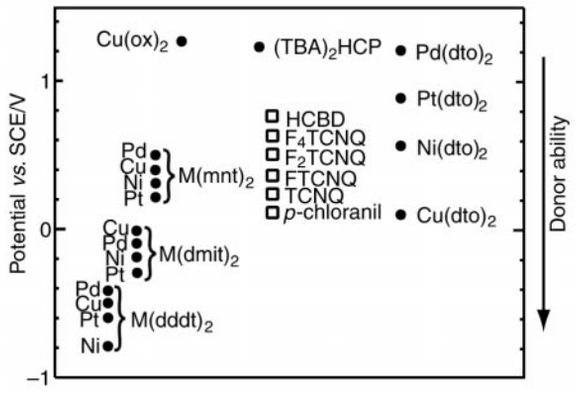


**Fig. 2** Oxidation potentials of $[M(L)_2]^{2-}$ and conventional electron acceptors. For L = ox or dto, the potential is the oxidation peak potential ($E_p^{ox}$). For L = dddt, dmit or mnt, it is the redox potential ($=(E_p^{ox}+E_p^{red})/2$ (refs. 32–34)). ● indicates the process of −2 to −1, □ indicates that of −1 to 0.

### 3.2 Redox properties of $[M(dto)_2]$

The redox properties of $(TPP)_2[M(dto)_2]$ and other acceptor and donor molecules determined by cyclic voltammetry are compared in Table 3 and Fig. 2. Since the redox process between $[M(dto)_2]^{2-}$ and $[M(dto)_2]^{-}$ was not reversible for M = Ni, Pd, or Pt, the peak potentials of the oxidation process $[M(dto)_2]^{2-} \rightarrow [M(dto)_2]^{-}$ are compared with the oxidation peak potentials of other chemical species.

The characteristic features regarding redox properties are summarized as follows. (1) It should be emphasized that $[M(dto)_2]^{2-}$ is much more easily oxidized than the oxalate analogue (+0.12 V for $[Cu(dto)_2]^{2-}$ *vs.* +1.33 V for $[Cu(ox)_2]^{2-}$). This indicates that the soft π orbitals and polarizable ligand dto contribute to the HOMO of $[M(dto)_2]^{2-}$ considerably. (2) The oxidation potential decreases in the order M = Pd > Pt > Ni > Cu, and the peak potentials of $[M(dto)_2]^{2-}$ are very sensitive to the central transition metal as shown in Fig. 2. The range of the potentials ($\Delta E$) is 1.09 V; from +1.21 V (M = Pd) to +0.12 V (M = Cu). Such a wide range is not found in the systems $[M(dddt)_2]^{2-}$ ($\Delta E = 0.38$ V),[32] $[M(dmit)_2]^{2-}$ ($\Delta E = 0.20$ V)[33] and $[M(mnt)_2]^{2-}$ ($\Delta E = 0.23$ V).[34] As demonstrated in Fig. 2, the redox potentials of other $[M(DTL)_2]^{2-}$ are less dependent on the central metals than are those of $M(dto)_2$.

It is of interest that a wide change of redox potential of $M(dto)_2$ can be achieved by replacing only the central metal without changing the molecular structure much. For conventional organic materials such as the TCNQs and *p*-benzoquinones, a wide change of redox property can only be achieved by replacing the substituent groups with those of considerably different Hammett σ value, *i.e.* $\Delta E \approx 0.7$ V for the TCNQ system (dicyano-TCNQ to tetramethyl-TCNQ) and $\Delta E \approx 1.7$ V for *p*-benzoquinone (*p*-cyanil to duroquinone). With these acceptors, a change of redox potential requires a major change of the molecular size compared to a minute change in the $M(dto)_2$ system. However, no fine tuning of redox potentials is possible for the $M(dto)_2$ system.

(3) A comparison with conventional organic acceptors in Fig. 2 revealed the following. $[Pd(dto)_2]^{2-}$ is a stable dianion as is $HCP^{2-}$. $[Pt(dto)_2]^{-}$ is a stronger acceptor by 0.15 V than HCBD which yields a fully ionic complex with TMTTF, a partially ionic one with $TTC_1$-TTF[35] and a neutral one with perylene.[36] Therefore it is expected that $[M(dto)_2]^{2-}$ (M = Pd or Pt) will be difficult to oxidize to the monoanion by the cation of conventional TTFs. The oxidation potential of $[Ni(dto)_2]^{2-}$ is located between those of $F_4TCNQ^{-\cdot}$ and $F_2TCNQ^{-\cdot}$, and it is possible to oxidize it to the monoanion state by an appropriate cation of TTFs. Since the oxidation potential of $[Cu(dto)_2]^{2-}$ is located below those of $FTCNQ^{-\cdot}$ and $TCNQ^{-\cdot}$ and close to that of the radical anion of *p*-chloranil, it may easily be oxidized to the monoanion state by a cation of conventional TTF derivatives.

### 3.3 Requirement for electron transfer from $[M(dto)_2]^{2-}$ to $TTFs^{+\cdot}$

Here, we discuss point (3) of the above summary in more detail. It is known for a 1:1 DA organic metal with low dimensionality that segregated stacking with a partial CT state is accessible when $-0.02 \leqslant \Delta E_{redox} \leqslant 0.34$ V, where $\Delta E_{redox}$ is the difference of redox potentials of D and A.[37] Full electron transfer ($D^{+\gamma}A^{-\gamma}$, $\gamma = 1$) occurs in the region of $\Delta E_{redox} < -0.02$ V. By taking the boundary of ionization as $\Delta E_{redox} = -0.02$ V for the $M(DTL)_2$ CT complexes, it is expected that an electron donor molecule, $[M(DTL)_2]^{2-}$, will donate an electron to an electron acceptor molecule, $TTF^{+\cdot}$ when $\Delta E_{redox} = \{E_p^{ox}([M(DTL)_2]^{2-}) - E_p^{red}(TTF^{+\cdot})\} < -0.02$ V, where $E_p^{ox}$ and $E_p^{red}$ are oxidation and reduction peak potentials, respectively. Some examples are known, *i.e.* $[M(mnt)_2]^{2-}$ (M = Pt or Ni) gave $[M(mnt)_2]^{-}$ salts with ET[38] in the region of $\Delta E_{redox} < -0.02$ V.

In the following, the ionicity of $M(dto)_2$ in a CT complex was estimated based on information on the ionicity of the donor, stoichiometry and magnetic measurements of the complex in addition to the optical and structural characterization of the acceptor.

## 4 Summary of charge transfer complexes of $M(dto)_2$

### 4.1 General

The CT complexes of $M(dto)_2$ were prepared by electrooxidation of donor molecules under a constant current (0.3–2.0 μA) for a period of 10–70 days in the presence of $K_2[M(dto)_2]$ + 18-crown-6 ether or $(TPP)_2[M(dto)_2]$ as supporting electrolyte using an H-shaped cell of 20 ml or an Erlenmeyer-flask type cell of 100 ml with 1–2 mm diameter Pt electrodes. Aromatic hydrocarbons (pyrene, perylene, naphthacene), hexamethoxytriphenylene, TTT and $M(dddt)_2$ (M = Ni or Pt) gave no solids, too small amounts of materials to characterize, or precipitation of only neutral donor molecules on the electrode, while TTF derivatives usually gave solid CT complexes though the yield of products was very poor. Table 4 summarizes the results of complex formation: solvent used, shape, stoichiometry, electrical conductivity and absorption bands in UV-VIS-NIR and IR spectra of the CT complexes of only ET, BO, TMTTF and OMTTF. For other donor molecules such as TMTSF, DBTTF and EDT-TTF complete sets of data have not been accumulated yet, since the yield was small. Furthermore, all the crystals prepared by the electrocrystallization method using our electrolyte of $Cu(dto)_2$ were found to include no $Cu(dto)_2$.

### 4.2 Complex formation using $(TPP)_2Cu(dto)_2$ and TTFs

ET, BO and EDT-TTF gave highly conductive complexes. Especially EDT-TTF gave two kinds of conductive complexes from different solvents (PhCN + $CH_3CN$ + ethanol (EtOH) and 1,1,2-trichloroethane (TCE) + EtOH). However, no characteristic absorption bands of $[Cu(dto)_2]^{2-}$ were present in the IR and UV-VIS-NIR spectra in all cases of the above mentioned donor molecules, hence the counter anion species are uncertain at present.

The ET complex showed metallic behavior with very weak temperature dependence down to 127 K ($\sigma_{RT} = 9$, $\sigma_{127\ K} = 13$ S cm$^{-1}$), below which it behaved as a semiconductor ($\varepsilon_a = 73$ meV). The BO complex was metallic with $\sigma_{RT} = ca.$ 200 S cm$^{-1}$ and $\sigma_{liq.N2} = ca.$ 600 S cm$^{-1}$ and retained metallic behavior down to 4.2 K. The EDT-TTF complex from PhCN + $CH_3CN$ + EtOH was a semiconductor with

**Table 4** Results of electrocrystallization of TTF derivatives with $M(dto)_2$ electrolytes (M = Ni, Pd, Pt or Cu)

| Donor | M[a] | Solvent[b] | Shape[c] | Ratio | $\sigma$[d]/S cm$^{-1}$ ($\varepsilon_a$/meV) | UV-VIS-NIR[e]/$10^3$ cm$^{-1}$ A | $C_{D2}$ | C | D | $[M(dto)_2]^{2-}$ | IR[e]/cm$^{-1}$ C=O |
|---|---|---|---|---|---|---|---|---|---|---|---|
| BEDT-TTF (ET) | Ni | PhCN + EtOH(MeOH) | Plate | 2 : 1 | $1.5\times10^{-5}$ (310) | — | 6.8 | 11.6 | 21.6 | 17.2, 27.1, 32.5 | 1585, 1048, 915 |
| | Pd-1 | PhCN + MeOH | Plate | 2 : 1 | $6.0\times10^{-3}$ (180) | — | 7.5 | 11.4 | 21.4 | 24.5, 35.4 | 1585, 1046, 910 |
| | Pd-2 | PhCN + MeOH | Block | 2 : 1 | $4.3\times10^{-4}$ (220) | — | 7.1 | 11.1 | 21.7 | 24.9, 35.1 | 1585, 1044, 908 |
| | Pd-3 | PhCN + MeOH | Block | 4 : 1 | $1\times10^{0}$ metal | 3.7 | — | 10.5 | 19.6 | 25.1, 35.0 | 1588, 1053, 922 |
| | Pt | $CH_2Cl_2$, PhCN | Plate | 2 : 1 | $5.0\times10^{-4}$ (270) | — | 7.4 | 11.5 | 21.0 | 22.7, 31.3 | 1581, 1042, 914 |
| | Cu | $PhNO_2$, PhCN | Plate | — | $10^{-1}$ metal | 2.9 | — | 9.8 | 22.9 | (16.7) | (1435, 1406, 1050) |
| BEDO-TTF (BO) | Ni | PhCN | Plate | 2 : 1 | $1.0\times10^{-5}$ (260) | — | 6.5 | 11.6 | 21.4 | —, —, 32.1 | 1587, 1052, 916 |
| | Pd | PhCN | Block | 2 : 1 | $1.0\times10^{-7}$ (250) | — | 7.3 | 11.0 | 20.6 | 25.0, 35.2 | 1585, 1050, 913 |
| | Pt | PhCN | Poly | — | | — | 7.7 | 11.5 | 22.6 | 22.6, 29.4 | 1578, 1049, 917 |
| | Cu | PhCN | Plate | — | $2\times10^{2}$ metal | 1.6 | — | 13.3 | 21.5 | (26.0, 31.9) | (1596, 1059) |
| TMTTF | Ni | $CH_3CN$, TCE | Powder | 2 : 1 | Insulator* | — | 11.5 | 17.6 | 23.8 | —, —, 33.3 | 1580, 1051, 917 |
| | Pd | TCE | Powder | — | $10^{-10}$* | — | 11.5 | 17.0 | 24.5 | 24.5, 35.5 | 1579, 1048, 912 |
| OMTTF | Ni | TCE, PhCN | Powder | 2 : 1 | Insulator* | — | 11.5 | 17.5 | 24.0 | —, —, 33.2 | 1585, 1053, 916 |
| | Pd | TCE | Powder | — | Insulator* | — | 10.7 | 17.1 | 25.3 | 25.3, 36.0 | 1584, 1052, 912 |
| | Pt | PhCN | Powder | — | Insulator* | — | 11.3 | 16.8 | 23.9 | 23.9 | 1596, 1051, 914 |

[a]Central metal of $M(dto)_2$ dianion; Pd-1, Pd-2, Pd-3 indicate 2 : 1 β phase, 2 : 1 γ phase and 4 : 1 phase, respectively. [b]DCE = 1,2-Dichloroethane, TCE = 1,1,2-trichloroethane. [c]Poly indicates polycrystals. [d]Room temperature conductivity; * indicates results on a compressed pellet sample. [e]In KBr pellet; the data in parentheses are not ascribable to $Cu(dto)_2$ dianion.

$\sigma_{RT} = 11$ S cm$^{-1}$ and $\varepsilon_a = 41$ meV on a compressed pellet sample, while that from TCE + EtOH was an insulator.

Despite the attractive features in the electrical conductivity, the crystal structures have not been solved yet owing to the poor quality of the crystals. A preliminary result indicated the following lattice parameters for the ET complex: $a = 7.849$, $b = 12.641$, $c = 6.035$ Å, $\alpha = 98.712$, $\beta = 100.766$, $\gamma = 74.269°$ and $V = 562.5$ Å$^3$. The crystals of BO complex did not give significant reflections. The EDT-TTF complex from TCE + EtOH contained Cu atoms but no dto species, with the following lattice parameters: monoclinic, $a = 7.286(1)$, $b = 12.141(4)$, $c = 28.547(4)$ Å, $\beta = 82.65(1)°$ and $V = 2504(1)$ Å$^3$. No lattice parameters could be obtained for the EDT-TTF complex from PhCN + $CH_3CN$ + EtOH.

We suppose that the electron transfer from $[Cu(dto)_2]^{2-}$ to $D^{+\cdot}$ occurred during the electrocrystallization resulting in the formation of $[Cu(dto)_2]^{-}$ which is known to be susceptible to light and easily decomposes.[39]

## 5 BEDT-TTF complex of $M(dto)_2$ (M = Ni, Pd or Pt)

### 5.1 Preparation and crystal structures of (BEDT-TTF)$_n$[M(dto)$_2$] ($n$ = 2 or 4)

$Pd(dto)_2$ gave four kinds of crystals. For example, 23 mg of ET were placed in one compartment and 42 mg of $(TPP)_2[Pd(dto)_2]$ in both compartments of an H-shaped cell under an inert atmosphere. 20 ml of purified PhCN were added to dissolve the supporting electrolyte and most ET. The ET solution was oxidized under a constant current of 0.5 μA for 3.5 weeks to yield 1.4 mg of black plates and 1.9 mg of black rhombic blocks. These two kinds of crystals were separated under a microscope. The former is the monoclinic 2 : 1 salt (β-phase) which hardly shows an EPR signal at RT. The rhombic blocks were further classified into three groups; one having narrow EPR linewidth ($\Delta H = ca.$ 10 G at RT) and the others having a wide one ($\Delta H = ca.$ 40 G at RT). The former actually contains two phases: triclinic 2 : 1 salt (α- and γ-phase) and the latter is the 4 : 1 complex. Since it is difficult to separate the α- and γ-phases of $(ET)_2[Pd(dto)_2]$ by the usual method, the magnetic data described below on a powder sample are those for the mixture of both phases.

The addition of MeOH into the solution and a use of highly concentrated solution of $(TPP)_2[Pd(dto)_2]$ favor the growth of the 4 : 1 complex. The triclinic 2 : 1 complex has been commonly obtained with M = Ni, Pd or Pt, but the monoclinic 2 : 1 and 4 : 1 complexes have been obtained only with M = Pd so far, even when changing the crystal growth conditions extensively. (During the preparation of this manuscript, the authors found that Schweitzer and co-workers have prepared a metallic 4 : 1 complex of $Ni(dto)_2$, very recently.[40]) The crystal data of these complexes are summarized in Table 5. The atomic parameters, along with the bond lengths and

**Table 5** Crystal data, data collection and reduction parameters of $(BEDT\text{-}TTF)_2[M(dto)_2]$ (M = Pd, Ni or Pt) and $(BEDT\text{-}TTF)_4[Pd(dto)_2]$

| | $(BEDT\text{-}TTF)_2[M(dto)_2]$ | | | | | |
|---|---|---|---|---|---|---|
| | M = Ni | Pd (α) | Pd (β) | Pd (γ) | Pt | $(BEDT\text{-}TTF)_4[Pd(dto)_2]$ |
| Formula weight | 1068.41 | 1116.13 | 1116.13 | 1116.13 | 1204.79 | 1933.58 |
| Crystal system | Triclinic | Triclinic | Monoclinic | Triclinic | Triclinic | Triclinic |
| Space group | $P\bar{1}$ | $P\bar{1}$ | $P2_1/c$ | $P\bar{1}$ | $P\bar{1}$ | $P\bar{1}$ |
| $a$/Å | 9.715(2) | 9.808(1) | 14.000(3) | 9.1000(7) | 9.097(1) | 12.818(4) |
| $b$/Å | 12.679(3) | 12.617(1) | 9.843(2) | 13.148(1) | 13.124(2) | 18.867(2) |
| $c$/Å | 8.320(2) | 8.3870(9) | 13.640(3) | 8.9930(7) | 8.949(2) | 7.627(1) |
| $\alpha$/deg | 108.12(2) | 107.391(7) | | 67.257(4) | 67.37(1) | 95.66(1) |
| $\beta$/deg | 111.95(2) | 112.572(8) | 100.10(3) | 91.603(5) | 91.71(1) | 102.99(2) |
| $\gamma$/deg | 79.22(2) | 78.912(6) | | 69.220(4) | 69.56(1) | 104.63(3) |
| $V$/Å$^3$ | 900.5(4) | 911.0(2) | 1850.6(7) | 910.60(1) | 907.3(3) | 1624.3(6) |
| $Z$ | 1 | 1 | 2 | 1 | 1 | 1 |
| No. of intensity measurements | 7216 | 3387 | 4369 | 3465 | 7381 | 8144 |
| No. of independent obsd. reflections | 6010 | 2895 | 1808 | 2703 | 3962 | 4969 |
| No. of refined parameters | 223 | 223 | 223 | 223 | 223 | 385 |
| $R$ | 0.061 | 0.044 | 0.067 | 0.037 | 0.068 | 0.035 |

angles of $[M(dto)_2]$ (M = Pd, Pt or Ni) and ET, are deposited as ESI.

All the crystal structures of the semiconductive 2:1 complexes are unique among the ET complexes so far known in the sense that the anions are separated from one another and each is isolated by being surrounded by six dimers of cations. They construct three-dimensional alternating stacks composed of dimerized donor cations and dianions. This kind of structure has not been obtained by utilizing oxalate analogues, $M(ox)_2$. The formation of the unique structure of $(ET)_2[M(dto)_2]$ may be ascribed to both the Coulomb attractive cohesion and the high-dimensional S···S intermolecular atomic network. On the other hand, the 4:1 complex is metallic and the crystal structure of it resembles those of the 4:1 complexes of $M(ox)_2$ (M = Pt or Cu).[11,15]

Table 6 compares the bond distances of an ET molecule of different charge and those in the $M(dto)_2$ complexes. The bond lengths *a* and *b* are more sensitive to the charge than those of *c* and *d* and they show an approximately linear relation to the charge. The charge of ET ($\gamma$) was estimated by two methods as follows. A plot of bond length against the charge was obtained for each bond (*a*, *b*, *c* and *d*) of the ET molecule of known charge (0, +1/2, +2/3, +1 and +2 in Table 6) as shown in Fig. 3. The charge was estimated by plotting the observed bond length for the corresponding bond in Fig. 3. Then the charges were averaged to represent the charge of ET, which is given in the 7th column in Table 6.

On the other hand, Guionneau *et al.* have proposed an empirical formula (eqn. 1) to estimate the charge of an ET molecule based on the bond lengths *a* to *d* of a number of ET complexes.[42]

$$\gamma = 6.347 - 7.463\delta, \quad \delta = (b+c) - (a+d) \qquad (1)$$

An estimate of $\gamma$ employing eqn. (1) is also presented in the 9th column in Table 6.

**5.1.1 $(BEDT\text{-}TTF)_2[Pd(dto)_2]$ (α-, β- and γ-phases).** *α-Phase.* Even though the estimated charge based on the bond length of ET using Fig. 3 and eqn. (1) is $0.78 \pm 0.1$ and 0.82, respectively, the IR, UV-VIS-NIR spectrum, the magnetic properties by EPR and SQUID measurements of the complex and the planar structure of $[Pd(dto)_2]$ confirmed that the $[Pd(dto)_2]$ molecule is in the diamagnetic dianion state.

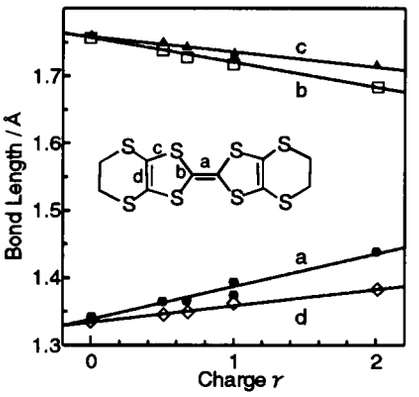


**Fig. 3** Plots of bond lengths (*a*, *b*, *c* and *d*) against the charge ($\gamma$) of a BEDT-TTF molecule.

Fig. 4 shows the crystal packing which is very similar to that of the $Ni(dto)_2$ complex described below. A nearly superimposed donor dimer has a shorter interplanar distance of 3.57 Å. The donor dimer and anion stack alternately along the *a* axis with their molecular long axes parallel to form a $D^{+\cdot}D^{+\cdot}A^{2-}$ column. The dihedral angle of the dimer and the anion molecular planes is *ca.* 70°. The $C_6S_8$ moiety of the ET molecule is in a boat form and the ethylene groups are eclipsed. The dashed lines in Fig. 4 indicate the intermolecular S···S atomic contacts shorter than the sum of the van der Waals radii (3.60 Å). Four short $S_{in}\cdots S_{in}$ atomic contacts exist within the nearly superimposed dimerized ET molecules, where $S_{in}$ is the inner S atom of an ET molecule. The dimer is connected to the neighboring anions to form an infinite $S_{out}\cdots S_a$ chain and neighboring chains are connected by short $S_{out}\cdots S_{out}$ contacts to each other, where $S_{out}$ and $S_a$ are the outer S atoms of an ET molecule and S atoms of

**Table 6** The bond length and charge ($\gamma$) of the BEDT-TTF molecule

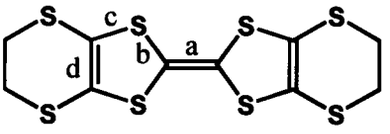


| | | Bond length/Å | | | | | | | |
|---|---|---|---|---|---|---|---|---|---|
| Complex[a] | $\gamma$ | *a* | *b*[b] | *c*[b] | *d* | $\gamma$[c] | $\delta$[d] | $\gamma$[e] | Ref. |
| $D^0$ | 0 | 1.312(12) | 1.757(8) | 1.754(8) | 1.332(12) | | 0.87 | 0.12 | 41 |
| | 0 | 1.343(4) | 1.756(3) | 1.760(3) | 1.333(4) | | 0.84 | 0.08 | 42 |
| $D_2(PF_6)$ | +1/2 | 1.365(4) | 1.740(2) | 1.750(2) | 1.345(3) | | 0.78 | 0.53 | 43 |
| $D_3(ClO_4)_2$ | +2/3 | 1.366(7) | 1.731(7) | 1.743(5) | 1.345(9) | | 0.76 | 0.68 | 44 |
| $D(PF_6)$ | +1 | 1.394(5) | 1.722(4) | 1.734(4) | 1.362(5) | | 0.70 | 1.12 | 45 |
| $D(ReO_4)(THF)_{0.5}$ | +1 | 1.375(28) | 1.719(10) | 1.729(10) | 1.365(18) | | 0.70 | 1.12 | 46 |
| $D(ClO_4)_2$ | +2 | 1.439(4) | 1.683(3) | 1.716(3) | 1.379(5) | | 0.58 | 2.02 | 47 |
| $D_2[Pd(dto)_2]$ (α) | | 1.374(8) | 1.725(6) | 1.740(6) | 1.351(8) | $0.78 \pm 0.1$ | 0.74 | 0.82 | |
| $D_2[Pd(dto)_2]$ (β) | | 1.37(3) | 1.733(19) | 1.746(19) | 1.36(3) | $0.72 \pm 0.25$ | 0.75 | 0.82 | |
| $D_2[Pd(dto)_2]$ (γ) | | 1.379(8) | 1.723(6) | 1.738(6) | 1.348(8) | $0.75 \pm 0.15$ | 0.73 | 0.90 | |
| $D_2[Ni(dto)_2]$ | | 1.391(6) | 1.720(5) | 1.738(5) | 1.361(6) | $0.9 \pm 0.1$ | 0.70 | 1.12 | |
| $D_2[Pt(dto)_2]$ | | 1.386(19) | 1.722(14) | 1.733(14) | 1.348(20) | $0.8 \pm 0.2$ | 0.72 | 0.97 | |
| $D_2[Pd(dto)_2]$ A | | 1.365(7) | 1.735(5) | 1.751(5) | 1.339(7) | $0.4 \pm 0.2$ | 0.78 | 0.53 | |
| $D_2[Pd(dto)_2]$ B | | 1.361(7) | 1.740(5) | 1.750(5) | 1.340(7) | $0.35 \pm 0.1$ | 0.79 | 0.45 | |

[a]D = BEDT-TTF. [b]The bond lengths *b* and *c* of $[M(dto)_2]$ complexes are the average of the chemically equivalent bonds, respectively. [c]$\gamma$ is the estimated charge of a BEDT-TTF molecule using relations between charge and bond length. For the bond lengths of $D^0$, the values of ref. 42 were used in the estimation of $\gamma$ of the $M(dto)_2$ complexes. [d]$\delta = (b+c)-(a+d)$. [e]$\gamma = 6.347 - 7.363\delta$ (ref. 42).

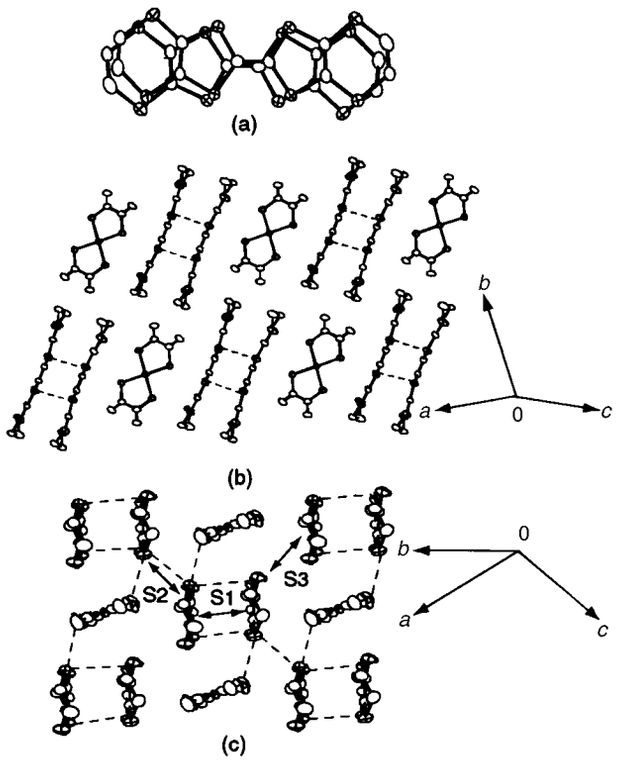


**Fig. 4** Crystal structure of $(BEDT\text{-}TTF)_2[Pd(dto)_2]$ (α-phase) and overlap pattern of BEDT-TTF molecules. (a) Overlap pattern of BEDT-TTF dimer with an interplanar spacing of 3.57 Å, (b) crystal structure viewed along the short axis of the donor molecule, (c) crystal structure viewed along the long axis of the donor molecule. Dashed lines indicate short S···S atomic contacts (⩽3.60 Å). The intermolecular overlap integrals (in $10^{-3}$) are $S_1=37.4$, $S_2=13.8$ and $S_3=8.5$.

dto ligand, respectively. Consequently a 3-D S···S network exists. Owing to the superimposed overlap, the intradimer overlap integral is the largest among the three 2:1 $Pd(dto)_2$ complexes discussed here ($S_1=37.4\times10^{-3}$). The outer S atoms contribute to the formation of short S···S contacts both between dimers and between dimer and anion. Owing to the small magnitude of the HOMO coefficient of the outer S atoms compared to that of the inner, the overlap integrals between dimers are rather small ($S_2=13.8\times10^{-3}$, $S_3=8.5\times10^{-3}$).

The packing style of the DDA along the molecular short axis of ET is depicted in Fig. 4(b). The torsion angle between the molecular long axis of ET and the direction of the $D^{+\cdot}D^{+\cdot}A^{2-}$ column is 77°.

*β-Phase.* The unit cell contains four ET molecules and two $[Pd(dto)_2]$ molecules. The large thermal parameters of C9 and C10, which are terminal ethylene carbon atoms of an ET molecule, may indicate disorder. The estimated charge of an ET molecule is $+0.72\pm0.25$ based on Fig. 3 and 0.82 using eqn. (1). These values indicate that the charge of $Pd(dto)_2$ is close to but less than −2. However, the IR, UV-VIS-NIR spectrum, the magnetic properties by EPR and SQUID measurements of the complex and the planar structure of $[Pd(dto)_2]$ confirmed that the $[Pd(dto)_2]$ molecule is in the diamagnetic dianion state. As a consequence it is concluded that no electron transfer takes place from $[Pd(dto)_2]^{2-}$ to $ET^{+\cdot}$ in the complex as expected on the basis of their redox properties.

As shown in Fig. 5, an ET molecule deforms as a boat shape. Both outer ethylene groups deviate from the averaged molecular plane as if two ET molecules encapsulate a dianion. The averaged molecular plane is calculated on the central $C_6S_8$ moiety, which is nearly flat. Two ET molecules form a dimer with a sliding overlap along the molecular long axis to avoid the steric hindrance of ethylene groups. The interplanar separation of the averaged molecular plane is 3.58 Å within a dimer. Dimerized ET molecules and a $[Pd(dto)_2]$ molecule construct a $D^{+\cdot}D^{+\cdot}A^{2-}$ stack along the *c* axis with their molecular long axes almost parallel. The dihedral angle between the averaged molecular planes of ET and $Pd(dto)_2$ is *ca.* 77° (Fig. 5c), while the torsion angle between the column direction and the long molecular axis of ET molecules is 77°.

Two short $S_{in}\cdots S_{in}$ contacts exist within a dimer (Fig. 5c). The calculated intradimer overlap integral ($S_1$) is $24.2\times10^{-3}$. A dimer is connected to the neighboring anions by three short S···S (two $S_{in}\cdots S_a$, one $S_{out}\cdots S_a$) contacts to form an infinite

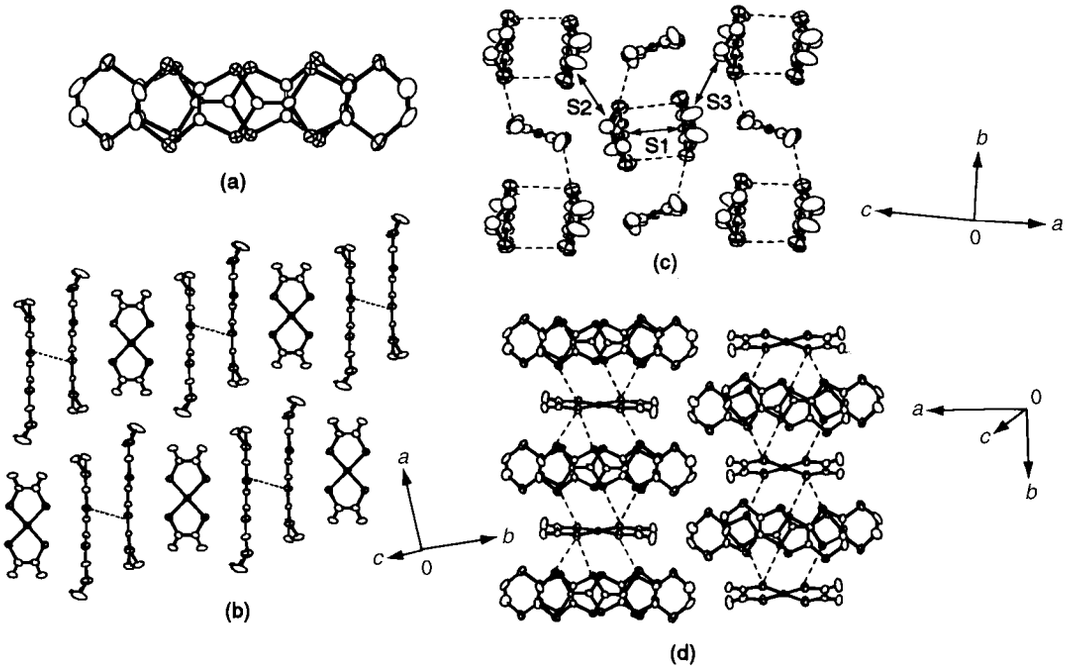


**Fig. 5** Crystal structure of $(BEDT\text{-}TTF)_2[Pd(dto)_2]$ (β-phase) and overlap pattern of BEDT-TTF molecules. (a) Overlap pattern of BEDT-TTF dimer with an interplanar spacing of 3.58 Å, (b) crystal structure viewed along the short axis of the donor molecule, (c) crystal structure viewed along the long axis of the donor molecule, (d) crystal structure projected on to the plane of the donor molecule. Dashed lines indicate short S···S atomic contacts (⩽3.60 Å). The intermolecular overlap integrals (in $10^{-3}$) are $S_1=24.2$, $S_2=13.8$ and $S_3=13.8$.

chain of S···S contacts as shown in Fig. 5(d), where three S atoms of only one side of an ET molecule contribute. The dimer is connected to the neighboring dimers by $S_{out}\cdots S_{out}$ contacts. As a result, 3-D S···S atomic contacts exist among the donor and anion molecules and give sizable interdimer overlap integrals: $S_2 = 13.8 \times 10^{-3}$ and $S_3 = 13.8 \times 10^{-3}$.

The orientation of the anion molecule is different from that of the α-phase, *viz.* though the neighboring $[Pd(dto)_2]$ molecules within a column are parallel, those in the neighboring columns tilt in a different way as shown in Fig. 5(c). As a result, the unit cell volume is about twice that of the α-phase.

*γ-Phase.* A charge of $+0.75 \pm 0.15$ or $+0.90$ was estimated based on Fig. 3 or eqn. (1), respectively. The stoichiometry, IR, EPR and SQUID measurements indicated a dianion state of $Pd(dto)_2$ that is consistent with the planar structure of $Pd(dto)_2$. It should be mentioned that the estimation of the charge of an ET molecule based on the structural data (Fig. 3, eqn. (1)) is not accurate enough and should be amended appropriately by the various kinds of physical measurements.

The crystal structure, packing pattern and donor overlap pattern (Fig. 6) are different from those in the α- and β-phases described above. The $ET^{+\cdot}$ molecules overlap with sliding in both directions of the molecular long and short axes as shown in Fig. 6(a) with an interplanar distance of 3.54 Å. The overlap mode is not a preferential one for the overlap integral which is the smallest ($S_1 = 3.5 \times 10^{-3}$) among the three 2 : 1 $[Pd(dto)_2]$ complexes of ET discussed here.

Donor dimers and anions form $D^{+\cdot}D^{+\cdot}A^{2-}$ columns with their molecular planes almost parallel. The dihedral angle of the donor and the anion molecular planes is *ca.* 4.1°. This parallel stacking of the constituent molecules within a column is similar to that observed in $(TTF)_2[Pd(dto)_2]$[20] and is a common one among the conventional donor and acceptor CT complexes, though the DDA, AAD or DDAA stack is rather rare.[48]

The $C_6S_8$ moiety of the ET molecule is almost flat and one of the ethylene groups extends toward the opposite direction of the plane to encapsulate a dianion by two ET molecules. There are no short intradimer and intracolumn S···S contacts. Instead, short S···S contacts exist between the DDA columns along the molecular short axes as shown in Fig. 6(c), (d). Though the overlap integral $S_2$ is negligible ($S_2 = -3.3 \times 10^{-3}$), $S_3$ is significantly large ($20.2 \times 10^{-3}$). There is no direct contact between anion molecules.

**5.1.2 $(BEDT\text{-}TTF)_2[Ni(dto)_2]$.** The estimated charge of an ET molecule is $+0.9 \pm 0.1$ using Fig. 3 while it is $+1.12$ using eqn. (1). These values demand that the $Ni(dto)_2$ is nearly dianionic. This is in good accordance with the optical spectra, which exhibit characteristic bands of $[Ni(dto)_2]^{2-}$, magnetic properties mentioned below, the 2 : 1 stoichiometry and the fact that the $[Ni(dto)_2]$ molecule has very similar bond angles and lengths to those in $K_2[Ni(dto)_2]$.[28] Therefore it is concluded that no electron transfer from $[Ni(dto)_2]^{2-}$ to $ET^{+\cdot}$ occurs during the electrocrystallization.

Fig. 7 shows the crystal packing of $(ET)_2[Ni(dto)_2]$, which resembles that of the 2 : 1 α-phase of $(ET)_2[Pd(dto)_2]$ including the eclipsed ethylene conformation of ET. A nearly superimposed donor dimer has an interplanar distance of 3.69 Å. All $[Ni(dto)_2]$ molecules are parallel to each other and there are no direct contacts among them. Owing to the superimposed overlap of ET molecules, the intradimer overlap integral $S_1$ is the largest among the five 2 : 1 complexes discussed here ($38.6 \times 10^{-3}$), even though the interplanar separation of the dimer is the largest. Other overlap integrals are rather small ($S_2 = 14.1 \times 10^{-3}$, $S_3 = 9.1 \times 10^{-3}$). The pattern of the S···S network and the relative orientation of constituent molecules (along the molecular long axis of ET, Fig. 7c) are almost the same as those in the α-$(ET)_2[Pd(dto)_2]$ complex including the length of the S···S contacts and dihedral angle between donor dimer and anion molecular planes.

**5.1.3 $(BEDT\text{-}TTF)_2[Pt(dto)_2]$.** The estimated charge of ET using the bond lengths is $+0.8 \pm 0.2$ based on Fig. 3 and $+0.97$ using eqn. (1). The monocation state of ET is also deduced based on its stoichiometry, IR, EPR and SQUID evidence and the very similar molecular structure of $Pt(dto)_2$ to that in $(TTF)_3[Pt(dto)_2]$.[20] Therefore no electron transfer from $[Pt(dto)_2]^{2-}$ to $ET^{+\cdot}$ occurs, as expected, during the electrocrystallization.

Fig. 8 presents the crystal structures, packing pattern and donor overlap pattern. All of them are similar to those observed in the 2 : 1 γ-phase of $(ET)_2[Pd(dto)_2]$. The interplanar distance of 3.52 Å was observed within an $ET^{+\cdot}$ dimer. Similar

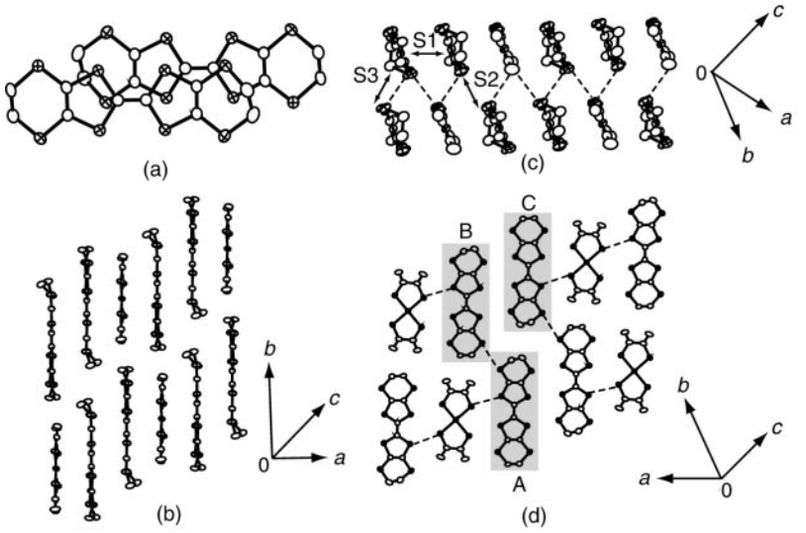


**Fig. 6** Crystal structure of $(BEDT\text{-}TTF)_2[Pd(dto)_2]$ (γ-phase) and overlap pattern of BEDT-TTF molecules. (a) Overlap pattern of BEDT-TTF dimer with an interplanar spacing of 3.54 Å, (b) two DDA columns viewed along the short axis of the donor molecule (A and C columns in (d)), (c) two DDA columns viewed along the long axis of the donor molecule (B and C columns in (d)), (d) crystal structure projected on to the plane of the donor molecule. Dashed lines indicate short S···S atomic contacts (≤3.60 Å). The intermolecular overlap integrals (in $10^{-3}$) are $S_1 = 3.5$, $S_2 = -3.3$ and $S_3 = 20.2$.

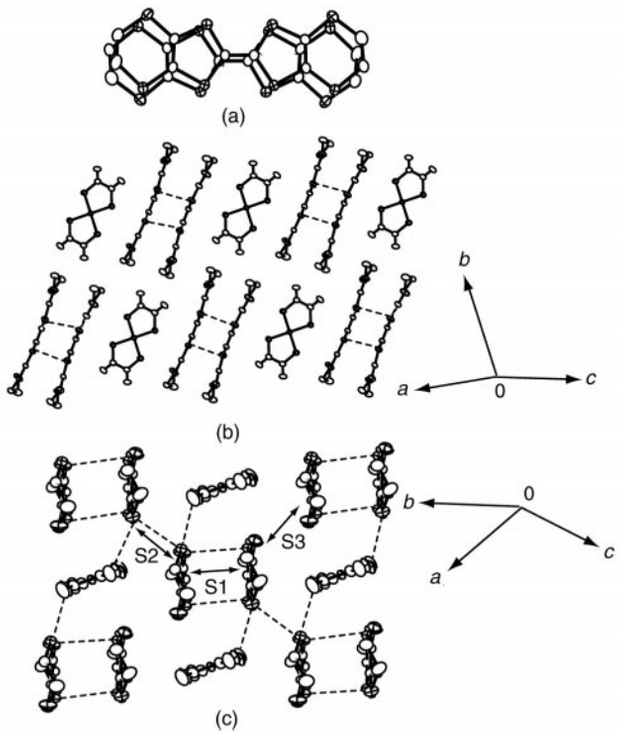


**Fig. 7** Crystal structure of $(BEDT\text{-}TTF)_2[Ni(dto)_2]$ and overlap pattern of BEDT-TTF molecules. (a) Overlap pattern of BEDT-TTF dimer with an interplanar spacing of 3.69 Å, (b) crystal structure viewed along the short axis of the donor molecule, (c) crystal structure viewed along the long axis of the donor molecule. Dashed lines indicate short S···S atomic contacts ($\leqslant$3.60 Å). The intermolecular overlap integrals (in $10^{-3}$) are $S_1=38.6$, $S_2=14.1$ and $S_3=9.1$.

to the γ-phase of the $Pd(dto)_2$ complex, the overlap integral $S_3$ is the largest ($S_1=2.4\times10^{-3}$, $S_2=-3.8\times10^{-3}$, $S_3=20.0\times10^{-3}$).

Donor dimers and anion molecules form $D^{+\cdot}D^{+\cdot}A^{2-}$ columns with a dihedral angle of *ca.* 4° between the donor and the anion molecular planes. No short intradimer and intracolumn S···S contacts were observed. Short S···S contacts exist between the DDA columns along the molecular short axes as depicted in Fig. 8(c), (d).

**5.1.4 $(BEDT\text{-}TTF)_4[Pd(dto)_2]$.** Two crystallographically independent ET molecules, A and B, exist. The estimated charge of ET using Fig. 3 is almost $+0.4\pm0.1$ for both kinds of ET molecules. Eqn. (1) also gives $\gamma=0.45$–$0.53$ for an ET molecule. The anion structure is very close to those in $(TTF)_2[Pd(dto)_2]$[20] and $(ET)_2[Pd(dto)_2]$. Therefore it is most likely that the $Pd(dto)_2$ is dianionic which is consistent with the IR, UV-VIS-NIR spectra and magnetic measurements as shown below. The $C_6S_8$ part deforms slightly as a boat shape with an eclipsed conformation of ethylene groups for A and a staggered one for B.

The crystal structure, packing pattern and donor overlap pattern are presented in Fig. 9. Two pairs of an AB dimer form a tetramer, which then makes a segregated column of $(ABBA)_n$ as seen in Fig. 9(a). The donor packing pattern (Fig. 9b) belongs to nearly the $ClO_4$ type ($\beta''_{412}$ type)[49] and is similar to those of $(ET)_4[Pt(ox)_2]$ (Fig. 9d) and $(ET)_4[Cu(ox)_2]$ which belong to the $ReO_4$ type.[12,13] The overlap patterns of AA, AB and BB are shown in Fig. 9(c). The interplanar distances between A and A, A and B and B and B are 3.77, 3.61, 3.97 Å, respectively.

Short atomic contacts only exist between the donor columns along the molecular short axis to construct a 2-D sheet of donor layer which is sandwiched by the anion layers as shown in Fig. 9(b). These features are very similar to those of the $[M(ox)_2]$ (M = Pd or Cu) salts.[11–13,15,16] However, in the 4 : 1 $[Pd(dto)_2]$ complex no tight atomic contacts are observed between the donor and the anion layers suggesting that the complex is structurally 2-D and the anions, in which two S and O atoms are out of the averaged molecular plane, are isolated.

Fig. 9(b) presents the overlap integrals; $a_1\approx a_2$, $p_1\approx p_3$, $q_1\approx q_3$. The calculated energy dispersion, Fermi surface and density of states (DOS) are summarized in Fig. 10(a). Four bands derived from the HOMO of four ET molecules weakly split into two sub-bands owing to the large separation between tetramers but no gap is formed between the sub-bands. The

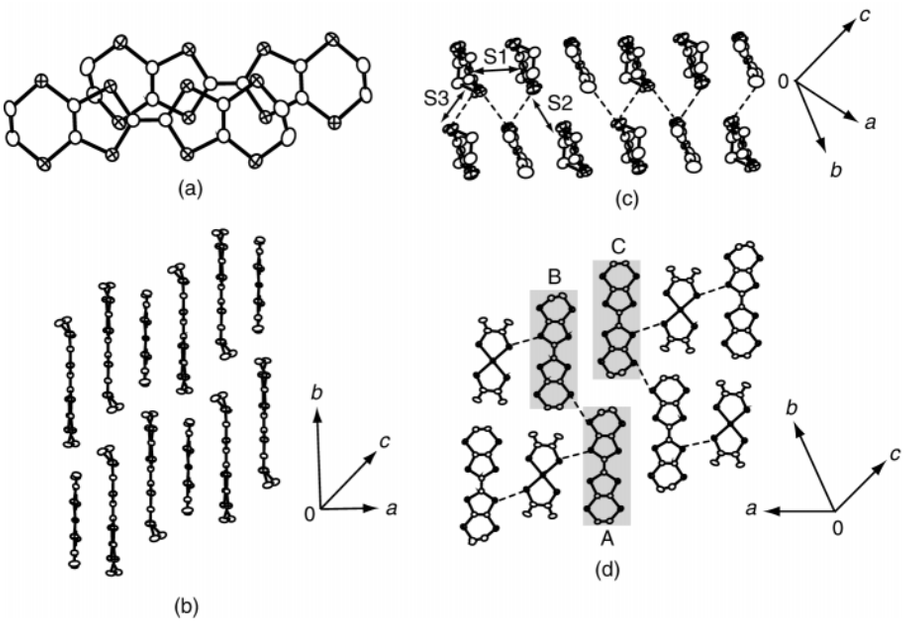


**Fig. 8** Crystal structure of $(BEDT\text{-}TTF)_2[Pt(dto)_2]$ and overlap pattern of BEDT-TTF molecules. (a) Overlap pattern of BEDT-TTF dimer with an interplanar spacing of 3.52 Å, (b) two DDA columns viewed along the short axis of the donor molecule (A and C columns in (d)), (c) two DDA columns viewed along the long axis of the donor molecule (B and C columns in (d)), (d) crystal structure projected on to the plane of the donor molecule. Dashed lines indicate short S···S atomic contacts ($\leqslant$3.60 Å).The intermolecular overlap integrals (in $10^{-3}$) are $S_1=2.4$, $S_2=-3.8$ and $S_3=20.0$.

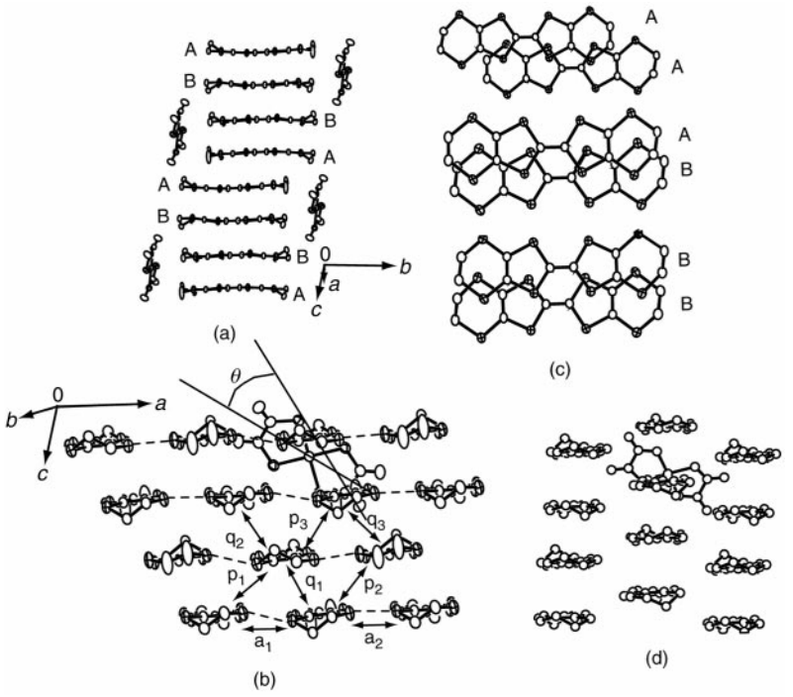


**Fig. 9** Crystal structure of $(BEDT\text{-}TTF)_4[Pd(dto)_2]$. (a) Crystal structure viewed along the short axis of the donor molecule, (b) crystal structure viewed along the long axis of the donor molecule, the intermolecular overlap integrals (in $10^{-3}$) being $a_1=-10.53$, $a_2=-9.78$, $p_1=16.20$, $p_2=11.50$, $p_3=-11.23$, $q_1=5.70$, $q_2=-4.81$, $q_3=-2.21$. Dashed lines indicate short S···S atomic contacts ($\leqslant 3.60$ Å). (c) Overlap pattern of BEDT-TTF molecules between the crystallographically equivalent (top and bottom) and different (middle) donor molecules. (d) Crystal structure of $(BEDT\text{-}TTF)_4Pt(ox)_2$ viewed along the long axis of the donor molecule for comparison.

lower sub-band has a wider dispersion than that of the upper one and a maximum of DOS appears in the upper part. The Fermi level bisects the upper narrow sub-band to make a small hole pocket around the Γ-point and an electron one around the M-point suggesting the semimetallic nature of this material with high DOS at the Fermi level.

As a comparison, the band dispersions, Fermi surfaces and DOSs of $(ET)_4[M(ox)_2]$ (M = Pt or Cu) using our parameters and reported crystal structures[11,15] are depicted in Fig. 10(b) and 10(c), respectively. The $ReO_4$-type packing of $ET^{+0.5}$ in $(ET)_4[M(ox)_2]$ yielded both 2-D hole pocket and 1-D electron-like Fermi surfaces by previous band calculations.[12,13,15,16] However, our calculated Fermi surfaces of the $M(ox)_2$ salts look considerably different from those reported. The $Pt(ox)_2$ complex has both 2-D hole- and electron-like pockets, while the $Cu(ox)_2$ complex has only hole-like pockets. Probably the different results are due to the fact that the Fermi level lies not only near the bottom of the highest HOMO band but also near the top of the second highest HOMO band. As a result, the Fermi surfaces calculated are very sensitive to the parameters used in the band calculation.

Nevertheless, we may compare the band parameters obtained solely by our band calculation between the $Pd(dto)_2$ and $M(ox)_2$ (M = Pt or Cu) complexes as follows. The calculated band width of $(ET)_4[Pd(dto)_2]$ ($W=0.90$ eV) is considerably smaller than those of $(ET)_4[Pt(ox)_2]$ (1.24 eV) and $(ET)_4[Cu(ox)_2]$ (1.09 eV), which is consistent with the poorer conductivity of the former ($\sigma_{RT}=4$–$8$ S cm$^{-1}$) than the last two ($\sigma_{RT}=20$ and 55 S cm$^{-1}$, respectively).

The main difference of the overlap integrals between $(ET)_4[Pd(dto)_2]$ and $(ET)_4[M(ox)_2]$ (M = Pt or Cu) stems from the packing patterns of the constituent molecules. The torsion angle between the dianion long axis and the stacking column of ET ($\theta$ in Fig. 9(b)) is 32° for $Pd(dto)_2$, 71° for $Pt(ox)_2$, and 66° for $Cu(ox)_2$, respectively. The longitudinal axes of the dianions are more or less parallel and perpendicular to the donor columns in the dto and ox materials, respectively. Among the interactions between ET molecules, the intracolumn one and the intercolumn one are more effectively related to the lengths of $M(dto)_2$ and $M(ox)_2$, as seen in Figs. 9(b) and 9(d), respectively. Moreover, the donor molecules overlap each other by sliding along the molecular short and long axes to form the columns in the former and latter complexes, respectively. As a result, the overlap integrals along the ET stacking column in the $Pd(dto)_2$ complex were suppressed to less than $6\times10^{-3}$ in absolute value ($q_1$–$q_3$ in Fig. 9(b)) from that of $10\times10^{-3}$ in $M(ox)_2$ complexes. Although the use of $M(dto)_2$ did not afford isostructural complexes to those of $M(ox)_2$, it reduced the intermolecular interaction between the donor molecules to produce the ET complex of high DOS at the Fermi level. The calculated value was 1.77 states eV$^{-1}$ molecule$^{-1}$ spin$^{-1}$ for the $Pd(dto)_2$ complex which is more than twice those of the $M(ox)_2$ complexes (0.70 states eV$^{-1}$ molecule$^{-1}$ spin$^{-1}$ for both M = Pt and Cu).

A preliminary measurement of thermoelectric power indicates that the Seebeck coefficient along the *c* axis is positive with $+16$ μV K$^{-1}$ at RT. It decreases linearly with temperature, crossing zero at around 220 K down to 150 K. Below 150 K the Seebeck coefficient decreases more rapidly ($-40$ μV K$^{-1}$ at 100 K). Along the *a* axis the Seebeck coefficient is $+8$ μV K$^{-1}$ and remains almost constant down to around 150 K, then decreases steeply below it, crossing zero at 100 K ($-70$ μV K$^{-1}$ at around 50 K). These complicated features of the temperature dependence of the thermoelectric power are characteristic for a semimetallic compound.

### 5.2 Optical properties of $(BEDT\text{-}TTF)_n[M(dto)_2]$ ($n=2$, M = Ni, Pd or Pt and $n=4$, M = Pd)

The electronic absorption spectra of all the 2 : 1 and 4 : 1 ET complexes are compared with that of the 1 : 1 Br salt of ET ($ET\cdot Br\cdot H_2O$) in Fig. 11. The absorption ascribable to the local excitations of $[M(dto)_2]^{2-}$ is indicated by arrows. The spectra indicate that only the 4 : 1 complex exhibits a characteristic band, which is labeled A in Fig. 11, extending below $5\times10^3$ cm$^{-1}$ and indicating both the partial CT state and the segregated stack of ET molecules in the crystal.

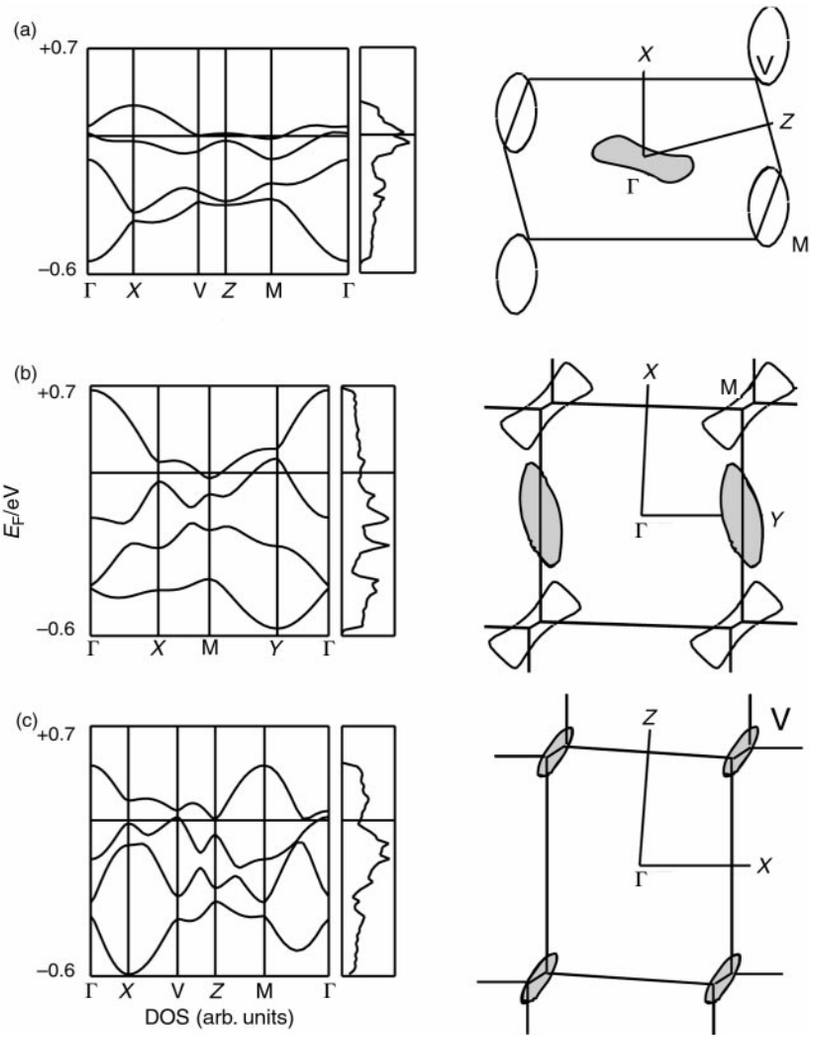


**Fig. 10** Energy dispersions, density of states (DOS) and Fermi surfaces calculated using crystal structures at room temperature. (a) (BEDT-TTF)$_4$[Pd(dto)$_2$], (b) (BEDT-TTF)$_4$[Pt(ox)$_2$], and (c) (BEDT-TTF)$_4$[Cu(ox)$_2$]. Hole pockets are shaded.

The origin of band A is usually interpreted by either an intraband transition in a metal or an intermolecular CT process from $D^0$ (or $A^{-\cdot}$) to $D^{+\cdot}$ (or $A^0$) for the charge separated case. For conventional CT complexes of TTF analogues, it appears below $5\times10^3$ cm$^{-1}$. Only in a rare system having extremely small on-site Coulomb repulsion, a low energy band appears from the CT process between $D^+$ (or $A^{-\cdot}$) molecules.[50]

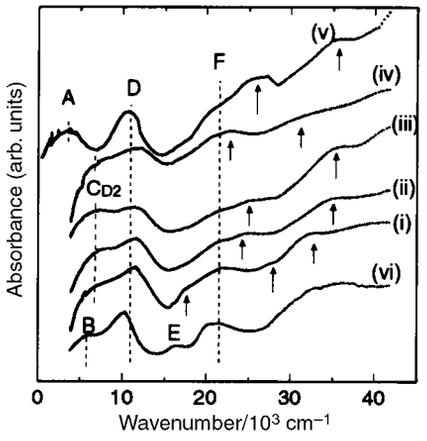


**Fig. 11** UV-VIS-NIR spectra of BEDT-TTF complexes of M(dto)$_2$ in KBr. The spectra of BEDT-TTF 2:1 complexes of [M(dto)$_2$] {(i) M = Ni, (ii) M = Pd (γ-phase), (iii) M = Pd (β-phase), (iv) M = Pt} and 4:1 complex of [Pd(dto)$_2$] (v) are compared with that of BEDT-TTF·Br·H$_2$O (vi). The bands ascribable to [M(dto)$_2$]$^{2-}$ are marked by arrows. For bands A, B, $C_{D2}$, D, E and F, see text.

The absence of band A in the 2:1 ET complexes studied here is in accordance with the integer CT state (+1.0) of ET molecules. The optical probe is much more effective in identifying the system having $\gamma=1$ than the bond-length analysis described in sections 5.1.1–5.1.3. Below $18\times10^3$ cm$^{-1}$ there are two bands with peaks at $(7–8)\times10^3$ and $(10–12)\times10^3$ cm$^{-1}$. These bands are commonly observed for these 2:1 complexes. Since the peak frequencies do not depend on the kinds of dianion used, both bands do not originate from the back CT, namely a transition associated with the electron transfer from [M(dto)$_2$]$^{2-}$ to $ET^{+\cdot}$. The transition energy of the lower energy band of the 2:1 complex is close to that of the lowest excitation band of ET·Br·H$_2$O, that is ascribed to the transition between the neighboring ET cation radicals: labeled B in Fig. 11. The band of the 2:1 complexes is located at slightly higher energy than B of ET·Br·H$_2$O and is certainly ascribed to the intradimer transition of the ET cation radicals, which is denoted $C_{D2}$.

The second band at $(10–12)\times10^3$ cm$^{-1}$, labeled D, is an intramolecular transition from the second HOMO to HOMO of $ET^{+\cdot}$ as discussed previously[51,52] and also from the following observations. (1) Dilute methanol solutions of ET cation radical salts of ET·Br·H$_2$O and (ET)$_3$(HSO$_4$)$_2$ exhibit absorption at $10.5\times10^3$ (D band), $(17–18)\times10^3$ (E band), and $23\times10^3$ cm$^{-1}$ (F band) associated with the ET cation molecule. (2) Although the interdimer overlap integrals of (ET)$_2$[M(dto)$_2$]

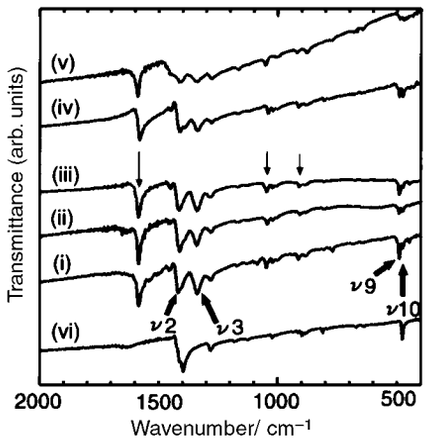


**Fig. 12** IR spectra of BEDT-TTF complexes of $M(dto)_2$ in KBr. The spectra of the 2 : 1 complexes {(i) M = Ni, (ii) M = Pd (γ-phases), (iii) M = Pd (β-phase), (iv) M = Pt} and 4 : 1 complex of $Pd(dto)_2$ (v) are compared with that of BEDT-TTF·Br·$H_2O$ (vi). The bands ascribable to $[M(dto)_2]^{2-}$ are marked by thin arrows and those to the $a_g$ mode of $BEDT\text{-}TTF^{+\cdot}$ by thick ones.

vary drastically from complex to complex, the observed intensity of the D band is insensitive to the kind of complex. Especially band D is clearly observed for the $[Pt(dto)_2]$ complex which has very small interdimer overlap integrals. Without considering some special mechanism of intensity borrowing, it is impossible to expect such a strong oscillator strength of band D in this complex if this were intermolecular.

The IR spectra of the 4 : 1 and all 2 : 1 ET complexes are compared with that of the 1 : 1 Br salt of ET in Fig. 12. The 2 : 1 complexes exhibit absorptions assignable to $M(dto)_2$ dianion, which are marked by thin arrows. Their frequencies summarized in Table 2 are not much different from those of $(TPP)_2[M(dto)_2]$, strongly suggesting the dianion state of $[M(dto)_2]$. No $a_g$ modes of $M(dto)_2$ are observed as expected based on the crystal structures.

Owing to the strong dimerization of donor cation molecules, the IR inactive $a_g$ mode of $ET^{+\cdot}$ appears in the spectra of these complexes as indicated by thick arrows in Fig. 12. These bands are observed at 1420 ($\nu_2$), 1340 ($\nu_3$), 491 ($\nu_9$) and 476 ($\nu_{10}$) for M = Ni, 1413, 1340, 490 and 477 for M = Pd, and 1412, 1338, 490 and 478 $cm^{-1}$ for M = Pt. The values are very similar to the reported values for $(ET\text{-}d_8)I_3$; 1401, 1331, 489 and 476 $cm^{-1}$.[53] So the IR spectra show excellent consistency with the results of the crystal structures and the electronic structures.

The IR spectrum of the 4 : 1 complex (curve v in Fig. 12) is similar to those of the 2 : 1 complexes except for both the presence of a peak at around 3500 $cm^{-1}$ (A band, not shown in Fig. 12) and more obscure features in the regions of 1400–1250 and 500–450 $cm^{-1}$. The $a_g$ mode of the ionized ET appears less pronouncedly at 1410, 1338, 486 and 471 $cm^{-1}$ while no $a_g$ mode of $Pd(dto)_2$ shows up in agreement with the crystal structure analysis.

### 5.3 Conductivity and magnetic properties of $(BEDT\text{-}TTF)_n[M(dto)_2]$ ($n = 2$, M = Ni, Pd or Pt and $n = 4$, M = Pd)

**5.3.1 Electrical conductivity of 2 : 1 complexes.** As expected, all the 2 : 1 complexes are insulators since ET molecules are monocationic and form dimers. The room temperature conductivities on single crystals are $1.5 \times 10^{-5}$, $4.5 \times 10^{-4}$, $6 \times 10^{-3}$ and $5 \times 10^{-4}$ S $cm^{-1}$ for the M = Ni or Pd (γ-phase), Pd (β-phase) and Pt complexes, respectively. From RT to 250 (M = Ni) or to 200 K (M = Pd or Pt) they show excellent linear Arrhenius plots with semiconductive activation energies of 0.31, 0.22, 0.18 and 0.27 eV, respectively.

We expected that the conduction should be related to the intermolecular overlap integrals. The overlap integrals of $S_1$–$S_3$ are not much different in magnitude between the complexes of $Ni(dto)_2$ and $Pd(dto)_2$ (α-phase) (Figs. 7 and 4, respectively). Compared to these values those of the complex of $Pt(dto)_2$ are small, especially for $S_1$ and $S_2$ (Fig. 8). Consequently we expected that $[Pt(dto)_2]$ would have the lowest conductivity with highest activation energy among the five complexes. However the conductivity seems to have no correlation with either the individual transfer integrals or the transition energies of band B (see Table 4). At this stage we are not able to explain rationally the above conductivity results based on the crystal and electronic structures of the complexes.

**5.3.2 Magnetic properties of 2 : 1 complexes.** Since the ET cation dimers form an alternating stack with the dianion of $[M(dto)_2]$, no localized magnetic moments are expected for both ET dimer site and $[M(dto)_2]$ site aside from the excited triplet moments from the singlet ground state within the ET dimers. The temperature dependence of magnetic susceptibility of the 2 : 1 complexes (M = Ni or Pd (mixture of α- and γ-phases), Pd (β-phase) and Pt complexes, respectively) was measured by SQUID at 0.1 or 0.5 T. The magnetic susceptibility $\chi_p$ was corrected by using the Pascal diamagnetic susceptibilities of $-5.54 \times 10^{-4}$, $-5.68 \times 10^{-4}$ and $-5.88 \times 10^{-4}$ emu $mol^{-1}$ for the complexes of $Ni(dto)_2$, $Pd(dto)_2$ and $Pt(dto)_2$, respectively (Fig. 13).

Curie paramagnetic behavior is observed at lower temperatures. The EPR measurements show that the spins ($g \approx 2.0$) are assignable to the isolated ET cation molecules as defect. The concentrations of the isolated $ET^{+\cdot}$ molecules are estimated as 4.9 (M = Ni), $2.5 \times 10^{-1}$ (M = Pd, α + γ), $4.9 \times 10^{-2}$ (M = Pd, β) and $3.2 \times 10^{-3}$% (M = Pt). Besides these localized spins at low temperatures on ET molecules, no signs of the existence of localized magnetic moments on $M(dto)_2$ were detected. The susceptibility observed at room temperature is $1.8 \times 10^{-4}$, $3.4 \times 10^{-4}$, $0.6 \times 10^{-4}$ and $5.7 \times 10^{-4}$ emu $mol^{-1}$ for the compounds of M = Ni or Pd (α + γ), Pd (β) and Pt, respectively.

An increase of susceptibility with increasing temperature is clearly observed in the M = Pd (α + γ) and Pt compounds but not in the M = Pd (β) and Ni compounds up to 350 K. The temperature dependence of observed $\chi_p$ can be interpreted by the singlet–triplet excitation mechanism expressed by eqn. (2)

$$\chi_p = \chi_0 + C/T + (2Ng^2\mu_B^2/k_BT)\{1/[3 + \exp(2J/k_BT)]\} \quad (2)$$

where $\chi_0$, $C$, $N$, $\mu_B$ and $k_B$ are the Pascal diamagnetism, Curie constant, Avogadro number, Bohr magneton and Boltzmann constant, respectively. The energy gap between the singlet ground state and triplet excited state is calculated as

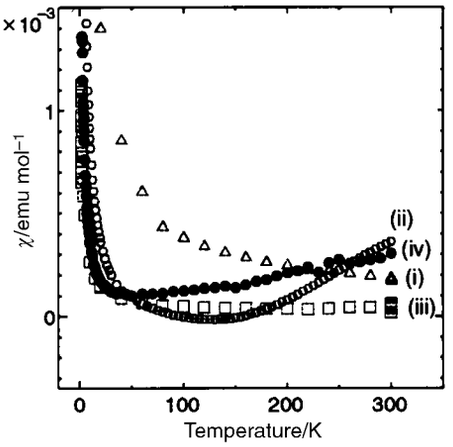


**Fig. 13** Temperature dependence of the magnetic susceptibility of $(BEDT\text{-}TTF)_2[M(dto)_2]$ (M = Ni (i), Pd (ii, α- and γ-phases), Pd (iii, β-phase) and Pt (iv)). The magnetic field was 5000 or 1000 G and no axis alignment was considered. The core diamagnetic contribution (Pascal diamagnetism) was subtracted.

$2J = -708\ \mathrm{cm}^{-1}$ for the Pt compound. For the Pd compound ($\alpha+\gamma$ phase), the concentration of the triplet excited state is too low to estimate a reliable $J$ value.

The EPR measurements on the 2 : 1 $Pd(dto)_2$ single crystal at RT indicate that the $\gamma$-phase exhibits thermally activated signals while the $\alpha$- and $\beta$-phases do not . The EPR intensities at RT are $3.3\times10^{-6}$ and $5.7\times10^{-4}$ emu $\mathrm{mol}^{-1}$ for the $\alpha$- and $\gamma$-phases, respectively, while almost no signal is detected for the $\beta$-phase. Accordingly, the data of M = Pd ($\alpha+\gamma$ phase) in Fig. 13 are ascribed to the $\gamma$-phase. The energy gap $2J$ is estimated as $-540\ \mathrm{cm}^{-1}$ from the temperature dependence of the EPR intensity of the $\gamma$-phase.

The energy gap may be related to the degree of dimerization of the ET molecules which can be scaled by the largest overlap integral among $S_1$ to $S_3$. The following order of overlap integral, $20.0\times10^{-3}$ (M = Pt) $\approx 20.2\times10^{-3}$ (M = Pd, $\gamma$) $< 24.2\times10^{-3}$ (M = Pd, $\beta$) $< 37.4\times10^{-3}$ (M = Pd, $\alpha$) $< 38.6\times10^{-3}$ (M = Ni), is qualitatively a good measure of the clear (for M = Pt, M = Pd, $\gamma$) and non-appearance (M = Pd, ($\alpha$, $\beta$) and M = Ni) of the singlet–triplet excitation, respectively.

**5.3.3 Electrical conductivity of 4 : 1 complex.** As mentioned, $(ET)_4[Pd(dto)_2]$ has the $ClO_4$-type ($\beta''_{412}$-type) crystal structure as do $(ET)_4M(CN)_4(H_2O)_n$ (M = Pt or Pd; $n = 0$ or 1),[23,54] which have afforded 2-D semimetallic electronic states. Even though $(ET)_4M(CN)_4$ (M = Pt or Pd) were semiconductors, $(ET)_2M(CN)_4(H_2O)$ had metal–insulator transitions at around 100 K and became superconducting under pressure ($T_c = ca.$ 1–2 K, at *ca.* 7 kbar).[23,54d,e] Fig. 14 shows the temperature dependence of the electrical resistivity of a single crystal of $(ET)_4[Pd(dto)_2]$ at ambient pressure. It shows metallic behavior down to 150 K with the conductivity at RT of 8 S $\mathrm{cm}^{-1}$ followed by a semiconductive dependence below 150 K. The conductivity at RT is much poorer than those of $(ET)_4M(CN)_4(H_2O)$ (M = Pd or Pt), which show $\sigma_{RT} = 100$–300 S $\mathrm{cm}^{-1}$. An Arrhenius plot yielded the activation energy of 20 meV between 100 and 50 K. A faint kink was observed at around 50 K. Even at 50 K the conductivity is fairly good ($\sigma_{50\ K} = ca.\ 8.35\times10^{-1}$ S $\mathrm{cm}^{-1}$). Below 50 K an Arrhenius plot indicated a gradual decrease of activation energy down to 4 K ($\sigma_{4\ K} = ca.\ 7.5\times10^{-4}$ S $\mathrm{cm}^{-1}$). However, it is still not certain whether the metallic state above 150 K is an intrinsic one or not.

**5.3.4 Magnetic properties of 4 : 1 complex.** In order to answer the inquiry evoked in the preceding section, an inspection of magnetic properties of this complex is necessary. However, due to the poor availability of the 4 : 1 complex, a reliable measurement for static magnetic susceptibility was not obtained. Therefore, we performed EPR measurements at ambient pressure. The shape of the signal is Lorentzian in the whole temperature region. The peak-to-peak linewidth ($\Delta H_{pp}$)

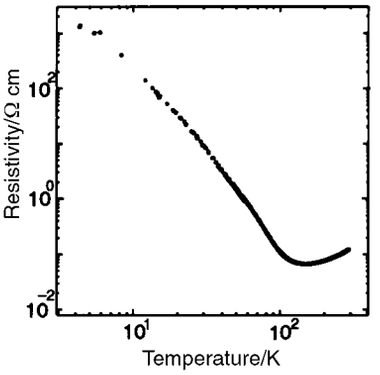


**Fig. 14** Temperature dependence of the electrical resistivity of (BEDT-TTF)$_4$[Pd(dto)$_2$].

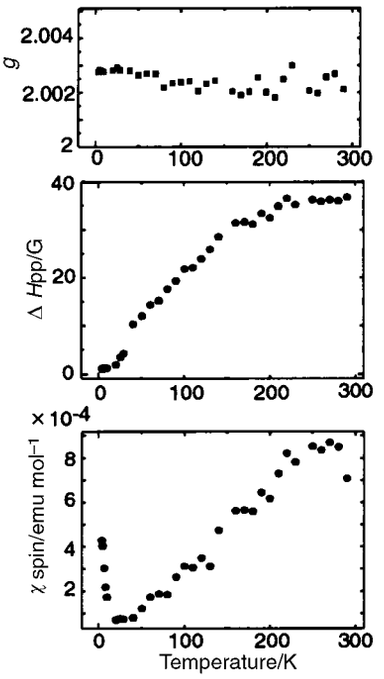


**Fig. 15** Temperature dependence of the $g$ value (top), linewidth $\Delta H_{pp}$ (middle), and spin susceptibility $\chi_{spin}$ (bottom) of (BEDT-TTF)$_4$[Pd(dto)$_2$] obtained from EPR measurements. The magnetic field was applied perpendicular to the BEDT-TTF molecular plane.

and the $g$ value show coincident angular dependence; namely they show a maximum, $\Delta H_{pp} = 53$ G and $g = 2.013$, when an external magnetic field ($H_0$) is nearly parallel to the ET molecular long axis and a minimum, $\Delta H_{pp} = 37$–38 G and $g = 2.003$, when $H_0$ is nearly perpendicular to the ET molecular plane. Fig. 15 shows temperature dependencies of the spin susceptibility $\chi_{spin}$, linewidth $\Delta H_{pp}$, and $g$ value with $H_0 \perp$ ET molecular plane.

The $\Delta H_{pp}$ decreases monotonically down to low temperatures. No distinct anomaly of $\Delta H_{pp}$ exists in the whole temperature range within the experimental error. The spin susceptibility is $8.3\times10^{-4}$ emu $\mathrm{mol}^{-1}$ at RT, then decreases as the temperature decreases, having a minimum at 50 K. The increase of the spin susceptibility below 50 K is well ascribed to the impurity-like Curie contribution. Curie-fitting below 50 K yields a Curie constant of $2.5\times10^{-4}$ (K emu $\mathrm{mol}^{-1}$), which corresponds to a spin concentration of $6.67\times10^{-2}$%. It should be noted that no drastic change in $\chi_{spin}$ is observed at around 150 K where the conductivity changes from metallic to semiconducting. The temperature dependence of $g$ exhibits no drastic anomaly at around 150 K, too. It stays in the range of 2.0018–2.0030 down to 150 K and increases very slightly toward 2.0021 ~ 2.0029 at low temperatures. So far the results in Fig. 15 do not indicate a distinct magnetic transition at 150 K.

The temperature dependencies of $\chi_{spin}$ and $\Delta H_{pp}$ in Fig. 15 are not consistent with the expected ones for a conventional metallic electronic state. The monotonic decrease of the intensity down to 150 K does not agree with the expected temperature independent Pauli paramagnetism as a simple metal. Although the monotonous decrease of the linewidth is consistent with the expected behavior from the Elliott mechanism for a metallic compound, both a further decrement of the linewidth even in the semiconductive region and no existence of a distinct kink at around 150 K are inconsistent with the temperature dependence of resistivity in Fig. 14.

Seemingly the magnetic properties suggest that the observed metallic state above 150 K is well characterized by the presence of thermally excited carriers, which is the typical behavior of a narrow-gap semiconductor. The activation-type fitting of the

spin susceptibility above 60 K by $\chi_{spin} = A \exp(-E_a/k_BT)$ yields an activation energy $E_a$ of 20 meV, which is in good agreement with that estimated from the Arrhenius fitting of the electrical resistivity between 50 and 100 K. By applying the theory developed by Epstein, Miller and Conwell for the temperature-dependent conductivity of a narrow-gap semiconductor such as *N*-methylphenazinium TCNQ,[55] the equation $\sigma = A(T)^{-a} \exp(-E_a/k_BT)$ with $a = 4.1$ and $E_a = 28.1$ meV well represents the observed conductivity at ambient pressure in Fig. 14 between 60 and 300 K. However, the system under discussion does not have structural disorder to localize spins. Instead, a localization of carriers by electron correlation is a more appropriate candidate since this system has a narrow band width compared to the effective on-site Coulomb repulsion energy ($U_{eff}$).

The inconsistency between the temperature dependencies of resistivity and magnetization is explained as follows. It is well known that the Pauli paramagnetic susceptibility of organic metals shows rather strong temperature dependence partly due to high thermal contraction of organic crystals. The $\chi_{spin}$ values decrease with decreasing temperature. That can be explained by the decrease of both DOS and $U_{eff}$ due to the increase of both transfer interactions and the Coulomb repulsion between neighboring sites by lattice shrinkage. The magnitude of the decrement of DOS and $U_{eff}$ differs from material to material. Among them, a semimetal suffers from a severe change of DOS and shows much stronger change of $\chi_{spin}$ with decreasing temperature than do metals having large Fermi surfaces. Since the Fermi level of the 4 : 1 complex is close both to the top of the second HOMO band and to the bottom of the first HOMO band, the area of the Fermi surface is expected to show strong temperature dependence. Therefore, it is quite natural for such a semimetallic compound having small Fermi surfaces to have strong temperature dependence of $\chi_{spin}$ even in the metallic regime. The temperature dependencies of $\chi_{spin}$ and $\Delta H_{pp}$ are very similar to those of a semimetal, $(ET)_4Pt(CN)_4 \cdot H_2O$, which exhibited metallic temperature dependence of resistivity down to *ca.* 70 K.[54] The close similarity in the magnetic and transport properties together with the semimetallic band structures between the 4 : 1 $Pd(dto)_2$ and $M(CN)_4 \cdot H_2O$ complexes strongly support the intrinsic metallic nature of the former complex above 150 K.

## 6 2 : 1 BEDO-TTF (BO) complexes of $M(dto)_2$ (M = Ni, Pd or Pt)

The BO molecule is known to be an excellent electron donor for the stable 2-D metals regardless of its counter components.[51a] Accordingly, $M(ox)_2$ (M = Pd or Cu) and $M(ox)_3$ (M = Fe, Cr or Al) afforded BO complexes metallic down to 1.8 K. However, $M(dto)_2$ (M = Ni or Pd) have afforded only insulators with BO so far.

**Table 7** Crystal data, data collection and reduction parameters of $(BEDO\text{-}TTF)_2[M(dto)_2]$ (M = Ni or Pd)

| | $(BEDO\text{-}TTF)_2[M(dto)_2]$ | |
|---|---|---|
| | M = Ni | M = Pd |
| Formula weight | 939.87 | 987.60 |
| Crystal system | Triclinic | Triclinic |
| Space group | $P\bar{1}$ | $P\bar{1}$ |
| *a*/Å | 9.736(3) | 9.757(2) |
| *b*/Å | 12.082(6) | 12.159(1) |
| *c*/Å | 7.317(2) | 7.385(2) |
| *α*/deg | 98.36(3) | 98.38(2) |
| *β*/deg | 111.26(2) | 111.20(2) |
| *γ*/deg | 91.85(3) | 92.01(2) |
| *V*/Å$^3$ | 790.2(5) | 804.5(3) |
| *Z* | 1 | 1 |
| No. of intensity measurements | 7472 | 5749 |
| No. of independent obsd. reflections | 1666 | 4447 |
| No. of refined parameters | 223 | 223 |
| *R* | 0.057 | 0.028 |

BO gave black plate-like and block-shaped single crystals with $Ni(dto)_2$ and $Pd(dto)_2$ in a ratio of 2 : 1. Their crystal data and the structural parameters are summarized in Table 7. They are isostructural. The unit cell contains two BO molecules and one $M(dto)_2$ molecule. The atomic parameters along with the bond angles and lengths have been deposited as ESI. The bond lengths and angles of $M(dto)_2$ are very similar to those of $M(dto)_2$ in the corresponding 2 : 1 ET complexes.

The ionization shift of the $b_{1u}$ $\nu_{31}$ IR band of a BO molecule is known to be large[56] and appeared at 1005–1007 cm$^{-1}$ for the $M(dto)_2$ (M = Ni, Pd or Pt) compounds. However, it is not reliable to estimate the charge of a BO molecule from the position of the $b_{1u}$ $\nu_{31}$ band as discussed in ref. 51(*a*). So we tried to estimate the $\gamma$ value of a BO molecule by a similar method to that described in section 3.1.

We have used the bond lengths of BO molecules in the BO compounds for which crystallographic analysis gave an *R* value less than 0.08 and no superlattices were detected. In a plot of bond lengths *a*, *b*, *c* or *d* against the charge of the BO molecule, the data of $\kappa\text{-}(BO)_2CF_3SO_3$ were excluded for our procedure since all its bond lengths deviate considerably from the correlation lines given by nine BO compounds: neutral BO ($\gamma = 0$), $(BO)_4(SQA^{2-})(H_2O)_6$ ($\gamma = 0.5$), $(BO)_2ClO_4$ ($\gamma = 0.5$), $(BO)_2ReO_4 \cdot H_2O$ ($\gamma = 0.5$), $(BO)_2(CHA^-)$ ($\gamma = 0.5$), $(BO)_2[MnBr_2(H_2O)]$ ($\gamma = 0.5$), $(BO)_2Br$ ($\gamma = 0.5$), $BO \cdot I_3$ ($\gamma = 1$) and $(BO)(I_3)_2$ ($\gamma = 2$). Furthermore, the bond length *d* of $BO \cdot I_3$ did not fit on the correlation line of *d vs.* charge of the BO molecule. This makes the estimation of charge of a BO molecule from a plot of $[(b+c)-(a+d)]$ *vs.* charge inaccurate. Hence, we used eqn. (3)

$$[(b+c)-a] = 2.154 - 9.047 \times 10^{-2}\gamma \quad (r = 0.970) \qquad (3)$$

obtained by a plot of $[(b+c)-a]$ *vs.* charge for the above 9 BO compounds to estimate the charge of BO complexes of $M(dto)_2$ as $\gamma = 0.99 \pm 0.20$ for M = Ni and $\gamma = 0.87 \pm 0.20$ for M = Pd. Even though the $\gamma$ values estimated from the bond lengths are not accurate enough, the IR and UV-VIS-NIR spectra and electric and magnetic properties strongly suggest that the $M(dto)_2$ molecules are in the dianion state and the BO molecule is fully ionized, *i.e.* +1. This charged state was confirmed by the Raman spectra (*vide infra*).

Fig. 16(a) shows the crystal structures of the 2 : 1 BO complexes of $Ni(dto)_2$ and $Pd(dto)_2$. Similar to $\alpha\text{-}(ET)_2[Pd(dto)_2]$ depicted in Fig. 4, a $BO^{+\cdot}$ dimer and dianion stack alternately to construct a $D^{+\cdot}D^{+\cdot}A^{2-}$ column along the (*c*–*a*) axis with their molecular long axes parallel. The dihedral angles of the dimer and the dianion molecules are *ca.* 55 and *ca.* 56° for the Ni and Pd compounds, respectively. These angles are considerably smaller than those observed in $(ET)_2[M(dto)_2]$ (*ca.* 70° for M = Ni, 71° for M = Pd (α) and 77° for Pd (β)). As shown in Fig. 16(b) the BO molecules overlap by sliding only along the molecular short axis and make short atomic contacts of CH···O between them. The angle between the flat $C_6S_4O_4$ plane of a BO molecule and the line which connects the centers of gravity of the donor molecules is *ca.* 60°. This angle together with the overlapping pattern in Fig. 16(b) is very common in many conductive BO complexes and originates from the peculiar self-assembling ability of the BO molecules.[51a,57] No short $S_{in}\cdots S_{in}$ atomic contacts exist within a dimer. However, short $S_{in}\cdots S_{in}$ contacts are seen between dimers.

In order to construct the segregated stack of BO molecules, the dimers should stack by themselves with the aid of atomic contacts of O···H and $S_{in}\cdots S_{in}$. However, in reality, an alternating stacking of $BO^{+\cdot}$ dimer and $M(dto)_2$ dianion is realized by insertion of a $M(dto)_2$ molecule between the BO dimers. Probably the static Coulomb attractive interactions

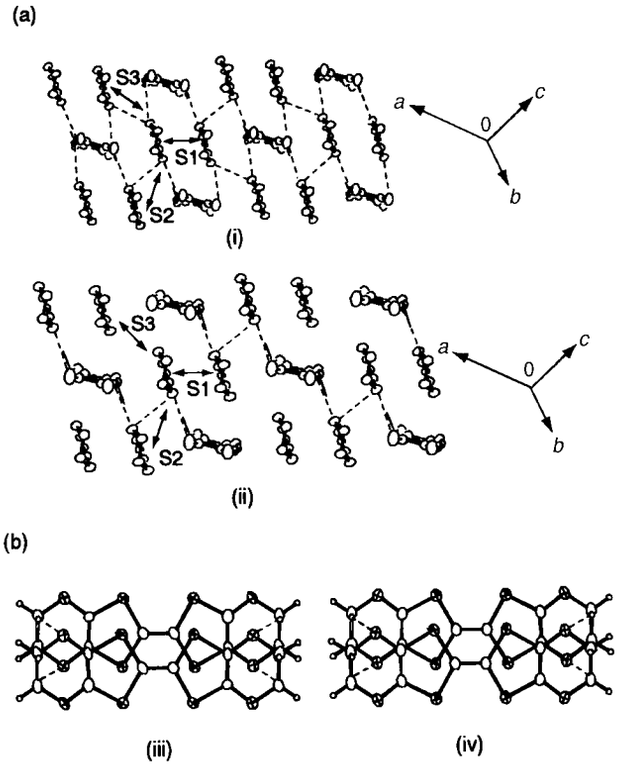


**Fig. 16** Crystal structures of (BEDO-TTF)$_2$[M(dto)$_2$]. (a) Crystal structure viewed along the long axis of the donor molecule. The short intermolecular contacts (S$\cdots$S$\leqslant$3.60, S$\cdots$O$\leqslant$3.32 Å) are indicated by dashed lines. (i) M = Ni. The intermolecular overlap integrals (in $10^{-3}$) are $S_1 = 0.25$, $S_2 = 19.4$, $S_3 = 11.4$. (ii) M = Pd. The intermolecular overlap integrals (in $10^{-3}$) are $S_1 = 0.18$, $S_2 = 17.0$, $S_3 = 10.8$. (b) Overlap pattern of the donor molecules in (BEDO-TTF)$_2$[M(dto)$_2$] (iii) M = Ni, (iv) M = Pd. The short intermolecular O$\cdots$H contacts ($\leqslant$2.72 Å) are indicated by dashed lines. The dihedral angles of the donor and M(dto)$_2$ molecular planes are 55 and 56° for M = Ni and Pd, respectively.

between (BO$\cdots$BO)$^{2+}$ and M(dto)$_2^{2-}$ and the short atomic $S_{in}\cdots S_a$ contacts between them as shown by the dashed lines in Fig. 16(a) are the driving forces of the stabilization of the alternating stack. Such alternating stacking of BO dimer and anion was also observed in BO·I$_3$ with a different pattern of $S_{in}\cdots S_{in}$ contacts.[58] The distances of the $S_{in}\cdots S_{in}$ contacts suggest that the [Pd(dto)$_2$] complex has slightly weaker intermolecular interactions compared to those of the [Ni(dto)$_2$] complex.

The overlap pattern of BO molecules is not a favorable one, owing to the phase problem of the HOMO, to gain large overlap integrals within a dimer. As a consequence, the overlap integral $S_1$ is about two orders of magnitude smaller than those between dimers ($S_2$, $S_3$), namely $S_1$, $S_2$ and $S_3$ are $0.25\times10^{-3}$, $19.4\times10^{-3}$ and $11.4\times10^{-3}$ for the Ni and $0.18\times10^{-3}$, $17.0\times10^{-3}$ and $10.8\times10^{-3}$ for Pd compounds, respectively. The overlap integrals of the [Pd(dto)$_2$] complex are a little smaller than the corresponding ones of the [Ni(dto)$_2$] complex in accordance with the strength of the $S_{in}\cdots S_{in}$ interdimer atomic contacts.

The static magnetic susceptibility of the [Ni(dto)$_2$] complex showed a Curie tail with Curie constant of $1.07\times10^{-3}$ K emu mol$^{-1}$ which corresponds to the Curie impurity of $2.85\times10^{-1}$%. A subtraction of Pascal diamagnetism ($-4.66\times10^{-4}$ emu mol$^{-1}$) clearly showed the singlet–triplet excitation expressed by eqn. (2) with $2J = -510$ cm$^{-1}$.

The UV-VIS-NIR and IR spectra of (BO)$_2$[M(dto)$_2$] (M = Ni or Pd) and the complex of Pt(dto)$_2$, the stoichiometry of which is not determined yet, are compared with those of the 1 : 1 complex of BO·I$_3$ in Figs. 17 and 18, respectively. There are no characteristic bands due to the partial degree of CT below $5\times10^3$ cm$^{-1}$. Consequently, the charge on a BO molecule is concluded to be an integer. Recently we have found that Raman spectroscopy is a fast and exact method to determine the $\gamma$ value of BO molecules in complexes.[59] Two totally symmetric C=C stretching modes ($\nu_2$ 1510–1660 cm$^{-1}$ and $\nu_3$ 1399–1530 cm$^{-1}$) were linearly dependent on the $\gamma$ values in the range of $\gamma = 0$–2 among the 19 CT complexes, as in eqns. (4) and (5)

$$\gamma = (1524.9 - \nu_3)/109.0 \quad (4)$$

$$\gamma = (1660.8 - \nu_2)/74.1 \quad (5)$$

with the possible error in $\gamma$ value of $\pm0.05$ and $\pm0.1$ from $\nu_3$ and $\nu_2$, respectively. Based on eqns. (4) and (5), the $\gamma$ value of BO was evaluated for the Pt(dto)$_2$ complex to be 1.00. Therefore, no electron transfer from [M(dto)$_2$]$^{2-}$ to BO$^{+\cdot}$ occurs during the electrocrystallization.

Owing to the dimerization, the $C_{D2}$ band appeared at $(6$–$8)\times10^3$ cm$^{-1}$, which includes both the intra- and inter-dimer transitions. The intra- and inter-dimer transitions are not separated well due to the overlap between the $C_{D2}$ band and the

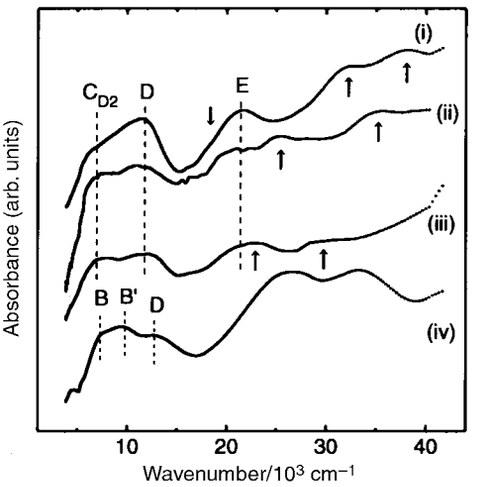


**Fig. 17** UV-VIS-NIR spectra of (BEDO-TTF)$_2$[M(dto)$_2$] {(i) M = Ni, (ii) M = Pd, (iii) M = Pt} in KBr compared with that of (BEDO-TTF)I$_3$ (iv). The bands ascribable to [M(dto)$_2$]$^{2-}$ are marked by arrows. For bands B, B′, $C_{D2}$, D and E, see text.

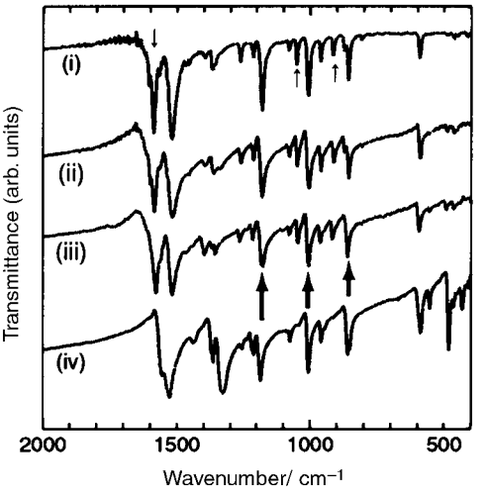


**Fig. 18** IR spectra of (BEDO-TTF)$_2$[M(dto)$_2$] {(i) M = Ni, (ii) M = Pd, (iii) M = Pt} in KBr compared with that of (BEDO-TTF)I$_3$ (iv). The bands ascribable to [M(dto)$_2$]$^{2-}$ are marked by thin arrows and those to the $a_g$ mode of BEDO-TTF$^{+\cdot}$ by thick ones.

band at (11–12) $\times 10^3$ cm$^{-1}$, which is the intramolecular transition of a $BO^{+\cdot}$ molecule (D band).[51a] In the case of $BO{\cdot}I_3$ (curve iv in Fig. 17), the intra- and inter-dimer transitions (B, B′) are seen rather clearly.[58] The intense $a_g$ mode of $BO^{+\cdot}$ appeared in the IR region at around 1178–1181, 1004–1007 and 856–860 cm$^{-1}$ as indicated by thick arrows in Fig. 18. The bands indicated by thin arrows in the figure are characteristic of $[M(dto)_2]^{2-}$. Therefore, the UV-VIS-NIR and IR spectra are good accordance with both the completely ionized component molecules and the structural features.

The single crystals of Ni and Pd complexes are insulators of the order of $10^{-5}$–$10^{-7}$ S cm$^{-1}$ with activation energies of 250–260 meV. In the case of the Pt complex, the small amount of the polycrystalline solid available hindered measurements of its stoichiometry and conductivity. Owing to the close similarity of IR, Raman and UV-VIS-NIR spectra of this complex to those of $(BO)_2[M(dto)_2]$ (M = Ni or Pd), it was presumed that the Pt complex has the same stoichiometry, electronic state and similar crystal structure to those of $(BO)_2[M(dto)_2]$ (M = Ni or Pd).

## 7 TMTTF and OMTTF complexes of $M(dto)_2$ (M = Ni, Pd or Pt)

TMTTF gave black powders with $Pd(dto)_2$ of low conductivity (*ca.* $10^{-10}$ S cm$^{-1}$). The $Ni(dto)_2$ also gave insulating powders. In Fig. 19 the IR spectra of $(TMTTF)_2[Ni(dto)_2]$ and the $[Pd(dto)_2]$ complex, the stoichiometry of which is not determined yet, are compared with that of TMTTF·Br. The characteristic bands ascribable to $TMTTF^{+\cdot}$ are observed at 1345, 935 and 498 cm$^{-1}$, which are indicated by thick arrows, in addition to those of $[M(dto)_2]^{2-}$ at 1579–1580, 1048–1051 and 912–917 cm$^{-1}$ indicated by thin arrows. According to the assignment of the IR bands of TMTTF radical cation,[60] the bands at 1345 and 498 cm$^{-1}$ are $a_g$ $\nu_4$ and $a_g$ $\nu_{10}$, respectively, and that at 935 cm$^{-1}$ is due to a C–C–H bending mode. The strong appearance of the $a_g$ mode evidences a non-uniform segregated state including dimerization of TMTTF cation molecules in the crystal.

Fig. 20 compares the UV-VIS-NIR spectrum of the $M(dto)_2$ complex (curve ii for M = Ni, curve iii for M = Pd) with that of TMTTF·Br (curve i). Evidently curves ii and iii are composed of those of $M(dto)_2^{2-}$ (indicated by arrows) and $TMTTF^{+\cdot}$ ($11.5 \times 10^3$, (17.0–17.6) $\times 10^3$, (23.8–24.5) $\times 10^3$ cm$^{-1}$). It should be noted that there is no optical band extending into the NIR region indicating that the complex is not in the mixed-valence state. The band at $11.5 \times 10^3$ cm$^{-1}$ is assigned to the

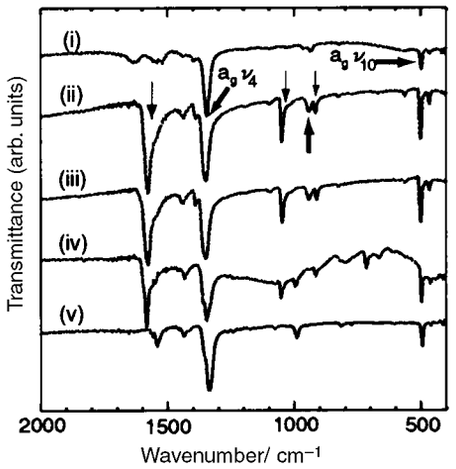


**Fig. 19** IR spectra of TMTTF complexes of Br (i) and $M(dto)_2$ ((ii) M = Ni, (iii) M = Pd), $(OMTTF)_2[Ni(dto)_2]$ (iv) and OMTTF·Br (v) in KBr. The bands ascribable to $[M(dto)_2]^{2-}$ are marked by thin arrows and those to the mode of $TMTTF^{+\cdot}$ by thick ones.

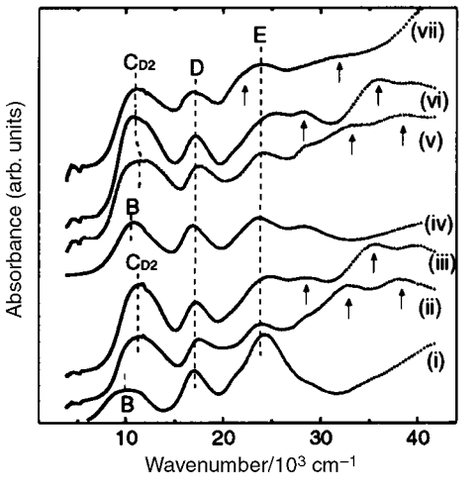


**Fig. 20** UV-VIS-NIR spectra of TMTTF and OMTTF complexes of $M(dto)_2$ (M = Ni, Pd or Pt) in KBr compared with those of TMTTF·Br and OMTTF·Br. Curves: TMTTF·Br (i), $(TMTTF)_2[Ni(dto)_2]$ (ii), $(TMTTF)_x[Pd(dto)_2]_y$ (iii), OMTTF·Br (iv), $(OMTTF)_2[Ni(dto)_2]$ (v), $(OMTTF)_x[Pd(dto)_2]_y$ (vi) and $(OMTTF)_x[Pt(dto)_2]_y$ (vii). The bands ascribable to $[M(dto)_2]^{2-}$ are marked by arrows. For bands B, $C_{D2}$, D and E, see text.

intradimer transition of TMTTF cation radicals as has been observed in $TMTTF{\cdot}CF_3TCNQ{\cdot}CH_3CN$ ($11.3 \times 10^3$ cm$^{-1}$, $C_{D2}$ band).[48i] This band has a little higher energy than the B band of TMTTF·Br (curve i, Fig. 20). The bands at (17.0–17.6) $\times 10^3$ and (23.8–24.5) $\times 10^3$ cm$^{-1}$ are due to the intramolecular transitions of $TMTTF^{+\cdot}$ (D and E band, respectively).

OMTTF also afforded $M(dto)_2$ (M = Ni, Pd or Pt) complexes for which the yield was enough to determine the stoichiometry of 2 : 1 only in the case of M = Ni. All of the complexes showed similar spectroscopic features to those of TMTTF complexes. In the IR spectra, a strong band at 1344–1347 cm$^{-1}$ and the characteristic bands of $M(dto)_2$ were observed along with some weak unassigned ones. Fig. 19 (curve iv) shows that of $(OMTTF)_2[Ni(dto)_2]$ as representative. Comparing to that of (OMTTF)Br (curve v in Fig. 19), the strong band should be assigned to the $a_g$ mode of $OMTTF^{+\cdot}$. Also, the spectra in the UV-VIS-NIR region were composed of the absorption bands of $OMTTF^{+\cdot}$ and $[M(dto)_2]^{2-}$. With the tentative assignments from the comparison to those of (OMTTF)Br, Fig. 20 (curves v–vii) shows the absorption spectra of OMTTF complexes. The very close similarity of the optical spectra among the five TMTTF and OMTTF complexes suggests the same charged state of each component molecule, similar stoichiometry, and similar molecular packing in the crystal. Furthermore, the close similarity of the spectra to those of 2 : 1 ET complexes of $M(dto)_2$ described above may support the dimerized state of the donor cations in these complexes. The highly dielectric nature of these complexes is consistent with the completely ionized donor dimers.

## 8 Summary

The preparation of charge transfer (CT) complexes of dithiooxalate (dto) transition metal salts $M(dto)_2$ (M = Ni, Pd, Pt or Cu) with BEDT-TTF (ET), BEDO-TTF (BO), OMTTF and TMTTF is described. The most characteristic feature of these solid CT complexes is that a donor cation dimer $D^{+\cdot}D^{+\cdot}$ and dianion ($A^{2-}$) of $M(dto)_2$ [M = Ni, Pd or Pt] construct $\cdots D^{+\cdot}D^{+\cdot}A^{2-}\cdots$ columns that is a unique packing among ET and BO compounds. Three different kinds of 2 : 1 complex were obtained between ET and $Pd(dto)_2$. The $M(dto)_2^{2-}$ are isolated from each other by being surrounded by six dimers of $D^{+\cdot}$ in the crystals three-dimensionally. The electronic absorption spectra and infrared

vibrational spectra indicated a characteristic intradimer transition at $(6–7)\times10^3\,cm^{-1}$ and $a_g$ modes of the donor cation dimer. Singlet–triplet magnetic excitation was clearly observed in some of them. The highly conductive complex $(ET)_4[Pd(dto)_2]$ was obtained, which showed semimetallic nature in its electrical and magnetic properties in accordance with band calculations.

## Acknowledgements

This work was in part supported by a Grant-in-Aid for Scientific Research from the Ministry of Education, Science, Sports, and Culture, Japan, a Grant for CREST (Core Research for Evolution Science and Technology) of Japan Science and Technology Corporation (JST) and a fund for "Research for Future" from Japan Society for Promotion of Science.

## References

1 L. Valade, M. Bousseau, A. Gleizes and P. Cassoux, *J. Chem. Soc., Chem. Commun.*, 1983, 110; L. Brossard, M. Ribault, M. Bousseau, L. Valade and P. Cassoux, *C. R. Acad. Sci., Ser. II*, 1986, **302**, 205.
2 E. A. Perez-Albuerne, L. C. Isett and R. K. Haller, *J. Chem. Soc., Chem. Commun.*, 1977, 417.
3 A. E. Underhill and M. M. Ahmad, *J. Chem. Soc., Chem. Commun.*, 1981, 67; A. Kobayashi, Y. Sasaki, H. Kobayashi, A. E. Underhill and M. M. Ahmad, *J. Chem. Soc., Chem. Commun.*, 1982, 390.
4 L. Alcacer and A. H. Maki, *J. Phys. Chem.*, 1974, **78**, 215; R. T. Henrique, L. Alcacer, J. P. Pouget and D. Jerome, *J. Phys. C*, 1984, **17**, 5197.
5 J. W. Bray, H. R. Hart, Jr., L. V. Interrante, I. S. Jacobs, J. S. Kasper, G. D. Watkins, S. H. Wee and J. C. Bonner, *Phys. Rev. Lett.*, 1975, **35**, 744.
6 J. S. Kasper, L. V. Interrante and C. A. Secaur, *J. Am. Chem. Soc.*, 1975, **97**, 890.
7 C. T. Vance, R. D. Bereman, J. Bordner, W. E. Hatfield and J. H. Helms, *Inorg. Chem.*, 1985, **24**, 2905; E. B. Yagubskii, A. I. Kotov, E. E. Laukhina, A. A. Ignatiev, L. I. Buravov, A. G. Khomenko, V. E. Shklover, S. S. Nagapetyan and Yu. T. Struchkov, *Mater. Sci.*, 1991, **17**, 55.
8 I. Hawkins and A. E. Underhill, *J. Chem. Soc., Chem. Commun.*, 1990, 1593.
9 A. E. Underhill, D. M. Watkins, J. M. Williams and K. Carneiro, in *Extended Linear Chain Compounds*, ed. J. S. Miller, Plenum, New York, 1981, vol. 1, p. 119.
10 K. Ueyama, G. Matsubayashi and T. Tanaka, *Inorg. Chim. Acta*, 1984, **87**, 143; K. Ueyama, A. Tanaka, G. Matsubayashi and T. Tanaka, *ibid.*, 1985, **97**, 201.
11 S. Görtner, I. Heinen, D. Schweitzer, B. Nuber and H. J. Keller, *Synth. Met.*, 1989, **31**, 199.
12 M.-H. Whangbo, J. Ren, W. Liang, J. P. Pouget, S. Ravy, J. M. Williams and M. A. Beno, *Inorg. Chem.*, 1992, **31**, 4169.
13 J. D. Martin, M.-L. Doublet and E. Canadel, *J. Phys. I*, 1993, **3**, 2451.
14 H. Tajima, S. Toyoda, M. Inokuchi and H. Kuroda, *Synth. Met.*, 1993, **55–57**, 2257.
15 X. Wang, C. Ge, X. Xing, P. Wang, D. Zhang, P. Wu and D. Zu, *Synth. Met.*, 1991, **39**, 355.
16 P. Wang, S. Bandow, Y. Maruyama, X. Wang and D. Zu, *Synth. Met.*, 1991, **44**, 147.
17 M. Kurmoo, A. W. Graham, P. Day, S. L. Coles, M. B. Hursthouse, J. L. Caufield, J. Singleton, F. L. Pratt, W. Hayes, L. Ducasse and P. Guionneau, *J. Am. Chem. Soc.*, 1995, **117**, 12209.
18 D. B. Brown and J. T. Wrobleski, *Molecular Metals*, NATO Conference, Les Arcs, 1978, p. 399, ed. W. E. Hatfield.
19 A. Gleizes, F. Clery, M. F. Bruniquel and P. Cassoux, *Inorg. Chim. Acta*, 1979, **37**, 19.
20 C. Bellitto, M. Bonamico, V. Fares, P. Imperatori and S. Patrizio, *J. Chem. Soc., Dalton Trans.*, 1989, 719.
21 G. Saito, K. Yoshida, M. Shibata, H. Yamochi, N. Kojima, M. Kusunoki and K. Sakaguchi, *Synth. Met.*, 1995, **70**, 1205.
22 K. Krogman, *Z. Anorg. Allg. Chem.*, 1968, **358**, 97.
23 H. Mori, I. Hirabayashi, S. Tanaka, T. Mori, Y. Maruyama and H. Inokuchi, *Solid State Commun.*, 1991, **80**, 411.
24 P. C. W. Leung, T. J. Emge, M. A. Beno, H. H. Wang, J. M. Williams, V. Petricek and P. Coppens, *J. Am. Chem. Soc.*, 1985, **107**, 6184.
25 E. G. Cox, W. Wardlaw and K. Webster, *J. Chem. Soc.*, 1935, 1475.
26 Crystan GM6.3, supplied by Mac Science, Japan, 1995, SHELXS 86, G. M. Sheldrick, University of Göttingen, Germany, 1986.
27 T. Mori, A. Kobayashi, Y. Sasaki, H. Kobayashi, G. Saito and H. Inokuchi, *Bull. Chem. Soc. Jpn.*, 1984, **57**, 627.
28 D. Coucouvanis, N. C. Baenziger and S. M. Johnson, *J. Am. Chem. Soc.*, 1973, **95**, 3875.
29 R. S. Czernuszewicz, K. Nakamoto and D. P. Strommen, *J. Am. Chem. Soc.*, 1982, **104**, 1515.
30 J. Fujita and K. Nakamoto, *Bull. Chem. Soc. Jpn.*, 1964, **37**, 528.
31 A. R. Latham, V. C. Hascall and H. B. Gray, *Inorg. Chem.*, 1965, **4**, 788.
32 C. T. Vance and R. D. Bereman, *Inorg. Chim. Acta*, 1988, **149**, 229; C. T. Vance, J. H. Welch and R. D. Bereman, *Inorg. Chim. Acta.*, 1989, **164**, 191, in dimethylformamide, *vs.* Ag/AgCl.
33 G. Steimecke, H. J. Sieler, R. Kirmse and E. Hoyer, *Phosphorus Sulfur Relat. Elem.*, 1979, **7**, 49, in $CH_3CN$, *vs.* SCE.
34 J. A. McCleverty, *Prog. Inorg. Chem.*, 1968, **10**, 84.
35 G. Saito, H. Kumagai, C. Katayama, C. Tanaka, J. Tanaka, P. Wu, T. Mori, K. Imaeda, T. Enoki, H. Inokuchi, Y. Higuchi and N. Yasuoka, *Isr. J. Chem.*, 1986, **27**, 319.
36 H. Yamochi, G. Saito, T. Sugano, M. Kinoshita, C. Katayama and J. Tanaka, *Chem. Lett.*, 1986, 1303; T. Ida, K. Yakushi, H. Kuroda, H. Yamochi and G. Saito, *Chem. Phys.*, 1991, **156**, 113.
37 G. Saito and J. P. Ferraris, *Bull. Chem. Soc. Jpn.*, 1980, **53**, 2141.
38 A. E. Underhill, J. S. Tonge and P. I. Clemenson, *Mol. Cryst. Liq. Cryst.*, 1985, **125**, 439.
39 T. Imamura, M. Ryan, G. Gordon and D. Coucouvanis, *J. Am. Chem. Soc.*, 1984, **106**, 984; M. G. Kanatzidis, N. C. Baenziger and D. Coucouvanis, *Inorg. Chem.*, 1985, **24**, 2680.
40 M. Schiller, W. Schmidt, D. Schweitzer, E. Balthes, H.-J. Koo, M. H. Whangbo, T. Klausa, I. Heinen, H. J. Keller and W. Strunz, International Symposium on Crystalline Organic Metals, Superconductors and Ferromagnets (ISCOM) '99, Oxford, UK, 1999.
41 H. Kobayashi, A. Kobayashi, Y. Sasaki, G. Saito and H. Inokuchi, *Bull. Chem. Soc. Jpn.*, 1986, **59**, 301.
42 P. Guionneau, C. J. Kepert, D. Chasseau, M. R. Truter and P. Day, *Synth. Met.*, 1997, **86**, 1973.
43 H. Kobayashi, R. Kato, T. Mori, A. Kobayashi, Y. Sasaki, G. Saito, T. Enoki and H. Inokuchi, *Chem. Lett.*, 1984, 759.
44 H. Kobayashi, R. Kato, T. Mori, A. Kobayashi, Y. Sasaki, G. Saito, T. Enoki and H. Inokuchi, *Chem. Lett.*, 1984, 179.
45 H. Kobayashi, R. Kato, T. Mori, A. Kobayashi, Y. Sasaki, G. Saito and H. Inokuchi, *Chem. Lett.*, 1983, 759.
46 H. Kobayashi, A. Kobayashi, Y. Sasaki, G. Saito and H. Inokuchi, *Chem. Lett.*, 1984, 183.
47 K. A. Abboud, M. B. Clevenger, G. F. de Oliveira and D. R. Talham, *J. Chem. Soc., Chem. Commun.*, 1993, 1560.
48 DAA stack: (*a*) S. Flandrois, P. Delhaes, J. Amiell, G. Brun, E. Torreilles, J. M. Fabre and L. Giral, *Phys. Lett.*, 1978, **66A**, 244; DDA stack: (*b*) S. Sakanoue, N. Yasuoka, N. Kasai and M. Kakudo, *Bull. Chem. Soc. Jpn.*, 1971, **44**, 1; (*c*) T. Inabe, N. Hoshino-Miyajima, I. Luneau, T. Mitani and Y. Maruyama, *Bull. Chem. Soc. Jpn.*, 1994, **67**, 622; DDAA stack: (*d*) A. Singhabhandhu, P. D. Robinson, J. H. Fang and W. E. Geiger, Jr., *Inorg. Chem.*, 1975, **14**, 318; (*e*) R. M. Metzger, N. E. Heimer, D. Gundel, H. Sixl, R. H. Harms, H. J. Keller, D. Nothe and D. Wehe, *J. Chem. Phys.*, 1982, **77**, 6203; (*f*) M. C. Grossel, F. Evans, J. A. Hriljac, K. Prout and S. C. Weaton, *J. Chem. Soc., Chem. Commun.*, 1990, 1494; (*g*) A. Dolbecq, M. Fourmigue and P. Batail, *Chem. Mater.*, 1994, **6**, 1413; (*h*) M. C. Grossel, P. B. Hitchcock, K. R. Seddon, T. Welton and S. C. Weston, *Chem. Mater.*, 1996, **8**, 977; (*i*) G. Saito, H. Ikegami, H. Yamochi, O. O. Drozova, T. Kondo, K. Nishimura, K. Ookubo, S. Horiuchi, M. Shibata, T. Nakamura and T. Akutagawa, to be submitted.
49 T. Mori, *Bull. Chem. Soc. Jpn.*, 1998, **71**, 2509.
50 (*a*) J. Dong, K. Yakushi and Y. Yamashita, *J. Mater. Chem.*, 1995, **5**, 1735; (*b*) K. Takimiya, A. Ohnishi, Y. Aso, T. Otsubo, F. Ogura, K. Kawabata, K. Tanaka and M. Mizutani, *Bull. Chem. Soc. Jpn.*, 1994, **67**, 766.
51 (*a*) S. Horiuchi, H. Yamochi, G. Saito, K. Sakaguchi and M. Kusunoki, *J. Am. Chem. Soc.*, 1996, **118**, 8604; (*b*) T. Senga, K. Kamoshida, L. A. Kushch, G. Saito, T. Inayoshi and I. Ono, *Mol. Cryst. Liq. Cryst.*, 1997, **296**, 97.

52 O. Drozdova, V. N. Semkin, R. M. Vlasova, N. D. Kushch and E. B. Yagubskii, *Synth. Met.*, 1994, **64**, 17.
53 M. E. Kozlov, K. I. Pokhodnia and A. A. Yurchenko, *Spectrochim. Acta, Part A*, 1989, **45**, 437.
54 (*a*) R. P. Shibaeva, R. M. Lobkovskaya, V. E. Korotkov, N. D. Kushch, E. B. Yagubskii and M. K. Makova, *Synth. Met.*, 1988, **27**, A457; (*b*) L. Ouahab, J. Padiou, D. Grandjean, C. G.-Lagrange, P. Delhaes and M. Bencharif, *J. Chem. Soc., Chem. Commun.*, 1989, 1038; (*c*) C. G.-Laglange, J. Amiell, E. Dupart, P. Delhaes, L. Ouahab, M. Fettouhi, S. Triki and D. Grandjean, *Synth. Met.*, 1991, **41–43**, 2053; (*d*) H. Mori, I. Hirabayashi, S. Tanaka, T. Mori, Y. Maruyama and H. Inokuchi, *Synth. Met.*, 1993, **55–57**, 2044; (*e*) T. Mori, K. Kato, Y. Maruyama, H. Inokuchi, H. Mori, I. Hirabayashi and S. Tanaka, *Solid State Commun.*, 1992, **82**, 177.
55 A. J. Epstein, E. M. Conwell, D. J. Sandman and J. S. Miller, *Solid State Commun.*, 1977, **23**, 355; A. J. Epstein and E. M. Conwell, *Solid State Commun.*, 1977, **24**, 627; J. S. Miller and A. J. Epstein, *Angew. Chem., Int. Ed. Engl.*, 1987, **26**, 287.
56 J. Moldenhauer, K. I. Pokhodnia, D. Schweitzer, I. Heinen and H. J. Keller, *Synth. Met.*, 1993, **55–57**, 2548.
57 F. Wudl, H. Yamochi, T. Suzuki, H. Isotalo, C. Fite, H. Kasmai, K. Liou, G. Srdanov, P. Coppens, K. Maly and A. Frost-Jensen, *J. Am. Chem. Soc.*, 1990, **112**, 2461.
58 S. Horiuchi, H. Yamochi, G. Saito and K. Matsumoto, *Mol. Cryst. Liq. Cryst.*, 1996, **284**, 357; S. Horiuchi, H. Yamochi and G. Saito, *ibid.*, 1997, **296**, 365.
59 O. Drozdova, H. Yamochi, K. Yakushi, M. Uruichi, S. Horiuchi and G. Saito, submitted to *J. Am. Chem. Soc.*
60 M. Meneghetti, R. Bozio, I. Zanon, C. Pecile, C. Ricotta and M. Zanetti, *J. Chem. Phys.*, 1984, **80**, 6210.

*Paper a908670f*